Spectroscopic Investigations Provide a Rationale for the Hydrogen-Evolving Activity of Dye-Sensitized Photocathodes Based on a Cobalt Tetraazamacrocyclic Catalyst

Sébastian Bold, Julien Massin, Emmanouil Giannoudis, Matthieu Koepf, Vincent Artero, Benjamin Dietzek, Murielle Chavarot-Kerlidou

▶ **To cite this version:**

Sébastian Bold, Julien Massin, Emmanouil Giannoudis, Matthieu Koepf, Vincent Artero, et al.. Spectroscopic Investigations Provide a Rationale for the Hydrogen-Evolving Activity of Dye-Sensitized Photocathodes Based on a Cobalt Tetraazamacrocyclic Catalyst. ACS Catalysis, 2021, 11 (6), pp.3662-3678. 10.1021/acscatal.0c05033 . hal-03190801

HAL Id: hal-03190801
https://hal.science/hal-03190801

Submitted on 18 Oct 2021

HAL is a multi-disciplinary open access archive for the deposit and dissemination of scientific research documents, whether they are published or not. The documents may come from teaching and research institutions in France or abroad, or from public or private research centers.

L'archive ouverte pluridisciplinaire **HAL**, est destinée au dépôt et à la diffusion de documents scientifiques de niveau recherche, publiés ou non, émanant des établissements d'enseignement et de recherche français ou étrangers, des laboratoires publics ou privés.

Spectroscopic investigations provide a rationale for the hydrogen-evolving activity of dye-sensitized photocathodes based on a cobalt tetraazamacrocyclic catalyst

Sebastian Bold,[a,b,c] Julien Massin,[†,a] Emmanouil Giannoudis,[a] Matthieu Koepf,[a] Vincent Artero,[a] Benjamin Dietzek[,b,c,d] and Murielle Chavarot-Kerlidou*[,a]*

a. Univ. Grenoble Alpes, CNRS, CEA, IRIG, Laboratoire de Chimie et Biologie des Métaux, 17 rue des Martyrs, F-38000 Grenoble, France.

b. Institute of Physical Chemistry and Abbe Center of Photonics, Friedrich Schiller University Jena, Helmholtzweg 4, 07743 Jena, Germany.

c. Department Functional Interfaces, Leibniz Institute of Photonic Technology Jena (Leibniz-IPHT), Albert-Einstein-Straße 9, 07745 Jena, Germany.

d. Center for Energy and Environmental Chemistry Jena (CEEC Jena), Friedrich Schiller University Jena, Philosophenweg 8, 07743 Jena, Germany.

Keywords.

Cobalt catalyst, dye-sensitized, solar fuels, photoelectrocatalysis, spectroscopy

Abstract.

Dye-sensitized photoelectrochemical cells (DSPECs) are a promising approach to produce solar fuels, e.g. by reduction of protons to molecular hydrogen. Here, we present functional NiO photocathodes sensitized with covalent organic dye-catalyst assemblies integrating a robust cobalt tetraazamacrocyclic complex. This catalyst proved to be decisive to improve the stability of these systems, hydrogen being produced with a 26-fold increase in turnover numbers compared to similar photocathodes based on a cobaloxime catalyst, all other conditions being strictly identical otherwise. Transient absorption spectroelectrochemical (TA-SEC) measurements observed the catalytically competent Co^{I} state in a functional dye-sensitized photocathode, with a lifetime of up to > 1 ms, comparable to the timescale of catalysis. They also unveiled the lack of efficiency of the thermally activated electron transfer from the reduced dye to the catalyst, which firstly limits the photocurrent density for hydrogen production. A second consequence is the accumulation of photogenerated charges on the acceptor side of the dye, ultimately leading to its degradation, as observed in operando and post-operando characterization of the system. This study thus provides tracks to improve the performances of hydrogen-evolving dye-sensitized photocathodes toward their integration into functional DSPECs.

Introduction

Storing solar energy, which by nature is intermittent, in chemical bonds, i.e. a solar fuel, is highly appealing to move from fossil fuels to renewable energies.[1] One promising approach to producing solar fuels relies on artificial photosynthesis, which mimics the natural photosynthetic process with synthetic components tailored to perform the desired redox reaction.[2–4] In that context, the production of hydrogen (H_2) in water splitting dye-sensitized photoelectrochemical cells (DSPECs) is the subject of intensive research efforts.[5,6] Tandem

DSPECs combine two photoelectrodes, a photoanode driving water oxidation to oxygen and a photocathode where protons and electrons are recombined to produce H_2, in that way mimicking the Z-scheme of natural photosynthesis.[7–9] However, the dye-sensitized photocathodes reported to date lag well behind their photoanode counterparts in terms of photocurrent density and stability and are the limiting factor in tandem DSPEC, calling for investigations to understand their limitations and to develop guidelines to improve their performances.[7–9]

Recently, molecular hydrogen-evolving catalysts based on first-row transition metals (Fe, Co, Ni) have been successfully integrated in dye-sensitized photocathodes.[7–27] In these studies, the synthetic tunability of the catalyst most of the time governs the electrode construction strategy: (i) immobilisation of supramolecular assemblies built by axial coordination of the dye on the Co center of a cobaloxime catalyst,[10,26] (ii) fully covalent dye-catalyst assemblies prepared thanks to a copper-catalyzed azide-alkyne cycloaddition (CuAAC) strategy using an azido-substituted cobalt diimine-dioxime complex,[14–16] (iii) layer-by-layer deposition of the dye and of a nickel bis(diphosphine) catalyst (Dubois type complex) functionalized with four phosphonate groups,[20–22] (iv) alternatively, co-immobilisation of dyes and catalysts at the semiconductor surface,[7–9,17–19,24,25] simplifying the synthesis and allowing to vary the dye/catalyst ratio. In addition to this diversity in the electrode architectures, which in turn strongly affects the electron transfer kinetics to the catalytic center, H_2 evolution activity was assessed under a wide range of conditions (nature of the electrolyte, pH, applied potential…). Altogether, this prevents direct comparison of the performances from one system to another to identify the best-performing components and to establish structure-activity relationships necessary for a rational improvement of the photocathode design.

In this study, we present a new noble metal-free covalent dye-catalyst assembly based on push-pull organic dyes covalently linked via CuAAC “click” chemistry to the tetraazamacrocyclic cobalt complex **Cat1** as catalytic unit. The superior activity and stability of the latter, compared

to the cobalt diimine-dioxime catalyst, was previously reported for photocatalytic proton reduction under fully aqueous conditions.[28–35] In parallel, the dye structure was modified from the previously published **T1-Co**[16] with a cyclopenta[1,2-b:5,4-b']dithiophene (CPDT) bridge to bathochromically shift the absorption and increase the extinction coefficient in the visible region.[36,37] The alkyl chains introduced on the linker are intended (i) to limit dyad-dyad interactions and (ii) to prevent dyad desorption by forming a hydrophobic layer at the surface of the NiO film.[38,39] Photoelectrochemical activity was assessed under strictly identical conditions to our previously-reported system,[16] thus providing a comprehensive comparison with **T1-Co**[16] and highlighting the beneficial role played by the **T2R** and **Cat1** moieties on the H_2 production performances. In addition, in-depth operando and post-operando characterizations of the **T2R-Cat1**-sensitized photocathode allowed to identify relevant degradation processes and to determine their kinetics. Finally, the light-driven formation of the different intermediates at the surface of the NiO film, including the catalytically competent Co^I state of **Cat1**, was investigated by transient absorption spectroelectrochemical (TA-SEC)[40–44] measurements and provided a mechanistic rational to improve the design of these dye-sensitized photocathodes.

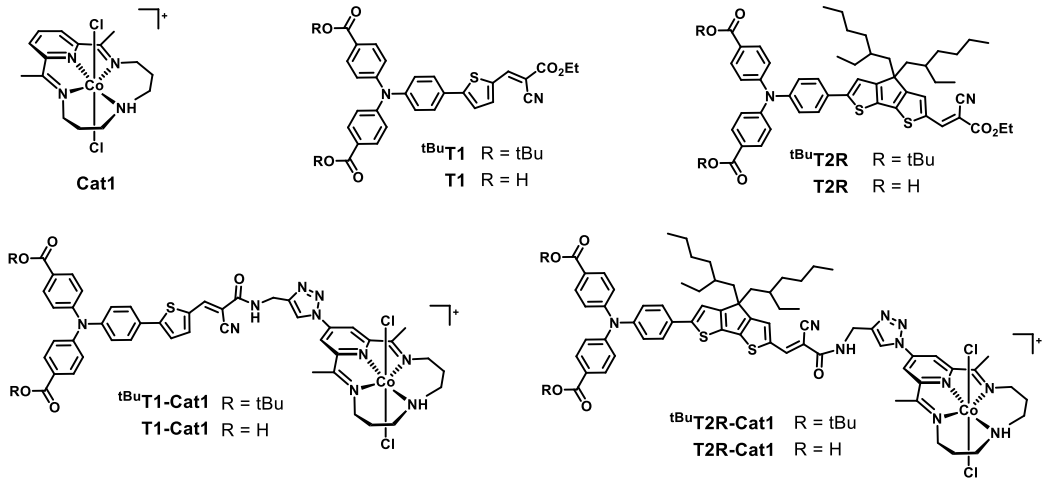

Figure 1. Structures of the H_2-evolving catalyst **Cat1**, the dyes **T1** and **T2R**, and the dyads **T1-Cat1** and **T2R-Cat1**.

Results

*Synthesis of the novel **Cat1**-based dyads*. Functionalization of **Cat1** is a challenging task, as reflected by the scarcity of procedures in the literature to prepare **Cat1** derivatives. Up to now, its catalytic performances were assessed either under electroassisted conditions[29,30,45] or under photocatalytic conditions in multicomponent homogenous systems.[29–35] The sole exception reported to date relies on a palladium-catalyzed cross-coupling introduction of a pyridine dicarboxylate anchoring group on the pyridine moiety of the ligand,[28] successfully allowing to assemble **Cat1** with quantum dots[28] or a TiO_2-protected silicon photoelectrode.[46] On the other hand, CuAAC is a highly versatile, efficient and modular coupling reaction. It was previously employed by some of us to assemble the push-pull organic dye **T1** (Figure 1) with the H_2-evolving cobalt diimine-dioxime catalyst Co(N^2,$N^{2\prime}$-propanediylbis(2,3-butandione-2-imine-3-oxime))Br_2 (**Co**), leading to the first functional noble metal-free NiO photocathode based on a covalent assembly.[16] We first decided to use the same strategy to covalently assemble **Cat1** with **T1** and with the novel **T2R** dye (Figure 1); however, all our attempts to prepare the cobalt complex **Cat1** substituted by an azido group in *para* position of the pyridine ring proved unsuccessful. An alternative route (Scheme 1) was thus developed: CuAAC coupling was first carried out between the alkyne-substituted dyes (**^{tBu}T1-alkyne** and **^{tBu}T2R-alkyne**, see SI) and the 4-azido-2,6-diacetylpyridine precursor (Scheme 1), followed by the templated synthesis of the tetraazamacrocyclic cobalt complex. This way, the targeted dyads were isolated in two steps under their *tert*-butyl ester protected forms (**^{tBu}T1-Cat1** and **^{tBu}T2R-Cat1**, Figure 1) in 50-60 % overall yield. Full synthetic details and characterizations are provided in the Supporting Information.

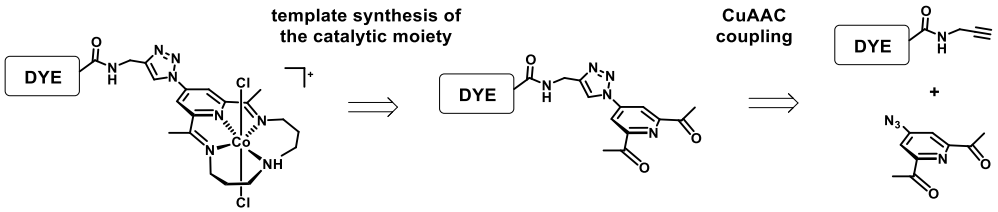

Scheme 1. Synthetic strategy for the preparation of **^{tBu}T1-Cat1** and **^{tBu}T2R-Cat1**.

Spectroscopic and electrochemical characterization in solution. All compounds were characterized by cyclic voltammetry (Table 1, Figures 2 & S1). The cyclic voltammogram of **^{tBu}T2R-Cat1** displays five redox events (Figure 2). On the anodic scan, two waves at +0.43 V and +0.58 V vs. $Fc^{+/0}$ are assigned to oxidation processes occurring on the dye moiety, by comparison with the cyclic voltammogram of **^{tBu}T2R** (Figure 2). The latter is characterized by two quasi-reversible waves at +0.48 V and +0.66 V vs. $Fc^{+/0}$, attributed to the oxidation of the triphenylamine (TPA) moiety and of the electron-rich CPDT bridge, respectively, as reported for related CPDT-based push-pull dyes.[36,47] On the cathodic scan of **^{tBu}T2R-Cat1**, the two reversible processes observed at –0.54 V and –0.97 V vs. $Fc^{+/0}$ are in full agreement with the two successive reversible reductions observed on the Co^{III} catalyst **Cat1** (Figure 2) yielding the formal Co^{II} and Co^{I} states, respectively.[30,33] The reduction of the acceptor part of the dye moiety is observed at –1.62 V vs. $Fc^{+/0}$ and shows a loss of reversibility compared to **^{tBu}T2R**. The cyclic voltammogram of **^{tBu}T1-Cat1** (Figure 2) displays very similar reduction processes for the catalyst (–0.53 V and –1.03 V vs. $Fc^{+/0}$) and dye (–1.65 V vs. $Fc^{+/0}$) units; the single anodic event at +0.64 V vs. $Fc^{+/0}$ is assigned to the TPA-centered oxidation process, by comparison with the cyclic voltammogram of **T1** (Figure S1a).[48,49]

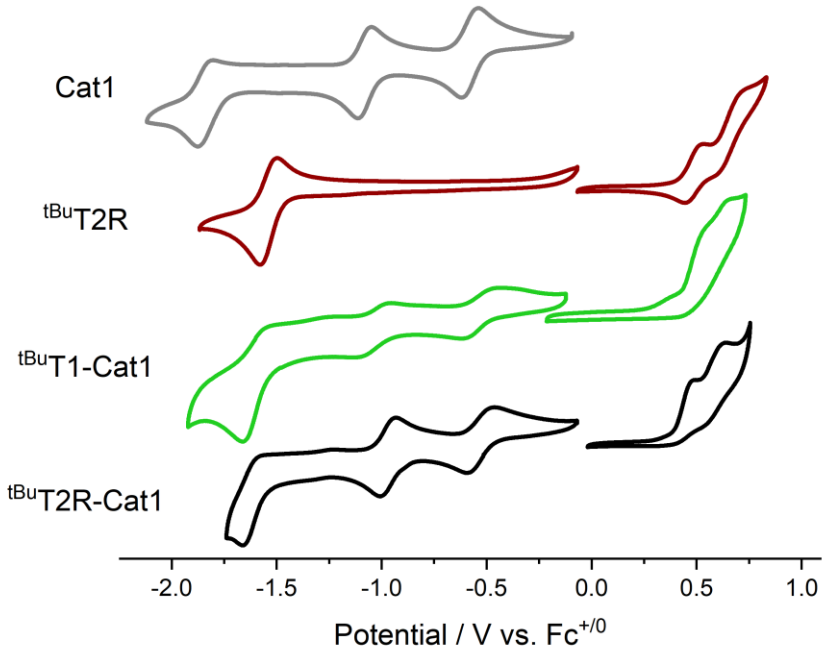

Figure 2. Cyclic voltammograms of **Cat1** (grey), **^{tBu}T2R** (red), **^{tBu}T1-Cat1** (green) and **^{tBu}T2R-Cat1** (black). CVs were recorded at 50 mV/s scan rate in 0.1 M $TBABF_4$ in dry DMF except for the reductive scan of **T1-Cat1,** in which TBACl was used as supporting electrolyte.

Table 1. Electrochemical potentials ($E_{1/2}$ in V vs. $Fc^{+/0}$) of investigated compounds determined by cyclic voltammetry.

Sample	$E_{dye}^{+/0}$	$E_{dye}^{2+/+}$	$E_{Co}^{III/II}$	$E_{Co}^{II/I}$	$E_{Co}^{I/0}$	$E_{dye}^{0/-}$ b)
Cat1	---	---	-0.58	-1.08	-1.84	---
^{tBu}T1	0.71	---	---	---	---	-1.52
^{tBu}T2R	0.48	0.66	---	---	---	-1.57
^{tBu}T1-Cat1	0.64 a)	---	-0.53	-1.03	---	-1.65
^{tBu}T2R-Cat1	0.43 a)	0.58 a)	-0.54	-0.97	---	-1.65

a) Peak potentials in the anodic scan.
b) Peak potentials in the cathodic scan.

The UV-Vis absorption spectra (Figure 3, Table S1) show two main absorption bands between 300 and 600 nm. The band at 350 nm is assigned to a π-π* transition on the TPA moiety[50] and its position remains unchanged for all dyads in comparison with the parent dye. At longer wavelengths, all compounds show the intramolecular charge transfer (ICT) transition from the TPA donor to the cyanoacrylate acceptor group, as typical for this class of push-pull dyes.[16,36,48] For the **^{tBu}T2R** series, this absorption is red-shifted in comparison to the **^{tBu}T1** series by ca.

0.33 eV (in ACN, Figure S2), which is attributed to the more extended conjugated system due to the CPDT linker. Furthermore, extinction coefficients for **^{tBu}T2R** (57,400 $M^{-1}cm^{-1}$, λ_{max} = 499 nm) exceed those of **^{tBu}T1** (27,700 $M^{-1}cm^{-1}$, λ_{max} = 448 nm).

Overall, in the covalent assemblies, the electrochemical and spectroscopic properties of the catalytic and dye units are retained, reflecting their electronic decoupling within the dyads, as previously established for **T1-Co**[16] and more generally frequently encountered for triazole-based dyads assembled by CuAAC coupling.[51–56]

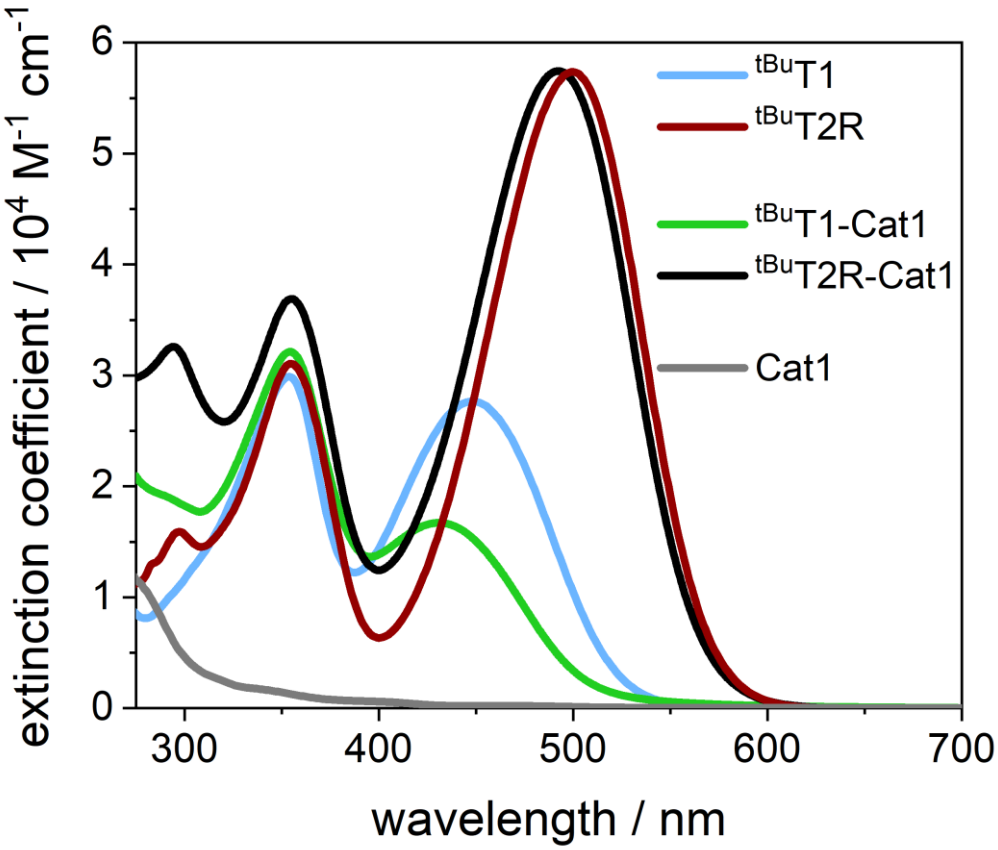

Figure 3. UV-Vis absorption spectra of **^{tBu}T1** and **^{tBu}T1-Cat1** in DMF and of **^{tBu}T2R**, **^{tBu}T2R-Cat1** and **Cat1** in MeOH.

NiO film sensitization and characterization. NiO films were prepared by spin-coating and sintering a F108 templated hydro-alcoholic $NiCl_2$ sol-gel.[16,57,58] The 4-layered films have a thickness of 880 ± 170 nm as determined by SEM (Figure S3, Table S2). They were sensitized by soaking for 24 h in methanolic solutions of the deprotected dyads (or dyes).

The amount of dyad (or dye) loading was quantified by dyad (or dye) desorption in a methanolic 1M phenylphosphonic acid solution followed by UV-vis absorption measurement of the resulting solution,[26,59] using the molar extinction coefficient of the TPA-centered band at 350 nm (Figure S4, Table S3). Grafting densities are in the range of 6-14 nmol·cm^{-2} (Table S4), in good agreement with the literature on other dye-sensitized NiO films.[14,16,26,48] We observed that the grafting density substantially varies from one batch of NiO films to another, preventing any straightforward analysis of the loading based on the molecular structures of the dyads. This supports the need to verify the grafting efficiency for each individual sample. For this, we used half of each freshly-sensitized NiO film to determine the dyad (or dye) loading while the other half was used for the assessment of photoelectrochemical hydrogen production. Hence, an accurate quantification of the amount of dyad grafted on the considered film was obtained and used to calculate the turnover number (TON) values for hydrogen production activity (see below).

Photoelectrochemical activity. The photoelectrochemical activity of the dye-sensitized NiO photocathodes was assessed in a three-electrode configuration setup under conditions identical to our previous studies[14,16,17,26] using an aqueous (*N*-morpholino)ethanesulfonic acid (MES) buffer solution at pH 5.5 as electrolyte; samples were irradiated with visible light at the equivalent of 1 sun intensity, using a 400 nm longpass filter and an IR filter. Linear sweep voltammograms (LSV) were recorded from +1.00 V to 0.00 V vs. RHE (Figure 4a). The large cathodic signal observed between +1.00 and ≈+0.6 V vs. RHE is attributed to capacitive charging of the NiO films.[60] Under irradiation, the dyad-sensitized NiO films start exhibiting cathodic photocurrents at ≈ +0.95 V vs. RHE, which are stable down to ≈ +0.5 V vs. RHE before increasing at more cathodic potentials. For the film sensitized with **T2R-Cat1**, the photocurrent reaches 13.5 μA·cm^{-2} at +0.14 V vs. RHE (dark current subtracted).

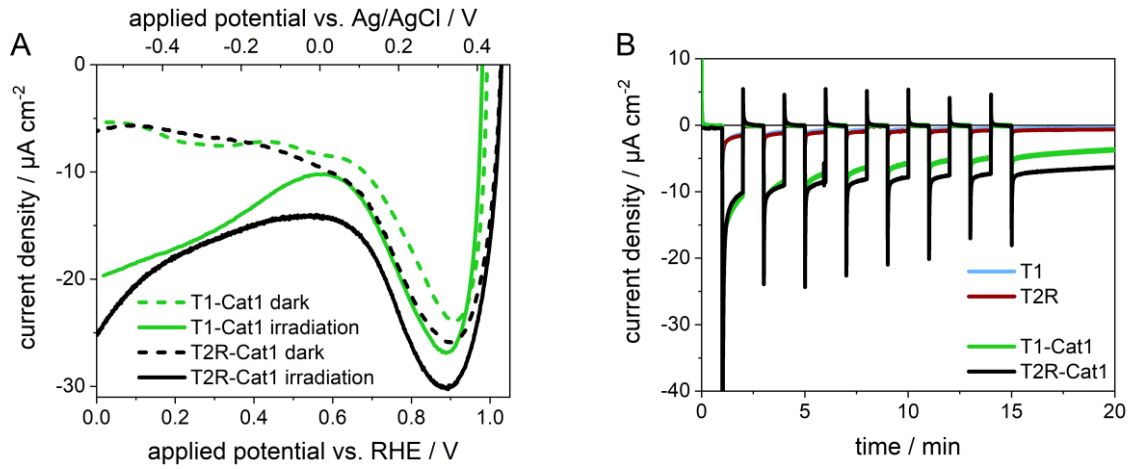

Figure 4. a) Linear scan voltammograms (LSV) of NiO films sensitized with the **Cat1** dyads recorded in the dark and under continuous visible light irradiation. b) Chopped-light chronoamperometric measurements recorded in aqueous 0.1 M pH 5.5 MES buffer at –0.4 V vs. Ag/AgCl (+0.14 V vs. RHE) on NiO films sensitized with the dyes and the **Cat1** dyads.

Chronoamperometric measurements under chopped light irradiation yielded insights into the magnitude and stability of the photocurrents measured at + 0.14 V vs. RHE, the potential applied for hydrogen production (Figure 4b). When light is turned on, the systems show an initial cathodic photocurrent spike; in addition, upon switching off the irradiation, a reverse anodic spike of lower intensity is observed, suggesting that some photogenerated electrons are accumulated on the dyad (see below) and not fully consumed by catalysis.[10,26,61] Importantly, almost no photocurrent is generated in the absence of the catalytic unit (–0.4 $\mu A \cdot cm^{-2}$ and –0.6 $\mu A \cdot cm^{-2}$ after 20 minutes for films sensitized with **T1** and **T2R**, respectively), while the presence of **Cat1** leads to a ten-fold increase of the photocurrent density (–3.7 and –6.3 $\mu A \cdot cm^{-2}$ for **T1-Cat1** and **T2R-Cat1**, respectively). In longer-term photoelectrochemical experiments under continuous light irradiation, all photocathodes show steady-state photocurrents (Figure 5, Figure S8), albeit with marked differences in photocurrent magnitude and stability over time. To investigate the role of the novel catalytic unit, the photoelectrochemical activity of the previously-reported dyad containing the cobalt diimine-dioxime catalyst Co(DO)(DOH)pnBr$_2$ (**T1-Co)** was reassessed, together with the activity of a novel dyad **T2R-Co** combining **T2R** with Co(DO)(DOH)pnBr$_2$ (see SI for synthesis and characterisations in Table S1, Figures S1b, S4-7). After normalisation of the photocurrent density to the amount of grafted dyad to compare

the intrinsic activity of the dyads (Figure 5b), the **Cat1** and **T2R** dyads showed slower decay in photocurrent and higher overall photocurrent than their **Co** and **T1** counterparts, respectively. On average, the **Cat1** dyads produced 3.2 times higher accumulated current than the **Co** dyads and the **T2R** dyads 1.7 times as much as the **T1** dyads, for a total 5.4-fold increase of **T2R-Cat1** over **T1-Co**.

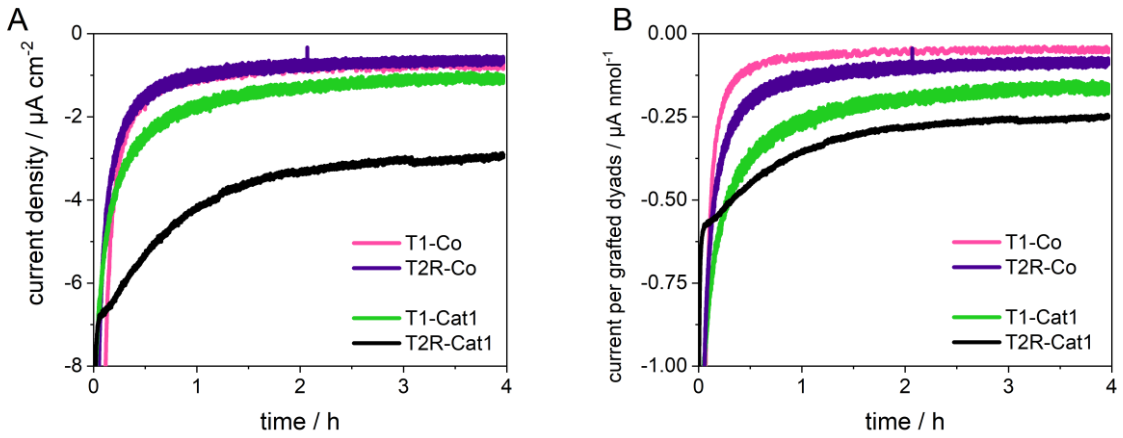

Figure 5. Photocurrents recorded on NiO films sensitized with the **Cat1**- and **Co**-based dyads during the first 4 hours of photoelectrochemical experiments (applied potential: +0.14 V vs. RHE). a) Absolute current density and b) current normalized to the amount of dyad grafted on the film, allowing to quantify the intrinsic activity of the dyads.

Hydrogen-evolving activity assessment. To confirm that the observed photocurrent originates from the reduction of protons into hydrogen, the H_2 evolution activity of the sensitized NiO photocathodes was assessed during long-term chronoamperometric experiments at an applied potential of +0.14 V vs. RHE and under continuous visible light irradiation. The amount of hydrogen produced was measured after 4 and 22 hours both in the headspace of the cell by gas chromatography and in the electrolyte using a micro Clark-type electrode probe following an established protocol.[14] Turnover numbers (TON_{Co}) were calculated, using the dyad loading quantified for the freshly sensitized film.

Table 2. Figures of merit of the different dyad-sensitized photocathodes determined from chronoamperometric measurements under continuous visible-light irradiation, in aqueous MES buffer electrolyte at pH 5.5, at an applied potential of +0.14 V vs. RHE (full set of experimental data in Table S4).

Sample	After 4 hours			After 22 hours		
	H_2 / (nmol·cm^{-2})	FE (%)	TON	H_2 / (nmol·cm^{-2})	FE (%)	TON
T1-Cat1	96 ± 14	65 ± 17	13 ± 1	162 ± 20	31 ± 4	23 ± 1
T2R-Cat1	187 ± 25	66 ± 7	21 ± 6	365 ± 122	39 ± 8	39 ± 8
T1-Co	11 ± 1	9 ± 1	0.7 ± 0.1	13 ± 4	3 ± 0	0.9 ± 0.3
T2R-Co	10 ± 2	11 ± 2	1.5 ± 0	10 ± 3	3 ± 2	1.5 ± 0.2

After 4 hours of irradiation, the **Cat1** dyads produced hydrogen with TON values of 13 ± 1 (**T1-Cat1**) and 22 ± 7 (**T2R-Cat1**) and Faradaic efficiencies around 65 % (Table 2). The activity of the **Co** dyads was much lower, with TON values below 2 and Faradaic efficiencies of ≈ 10 %, in agreement with previous reports.[14,16,17] Comparing the influence of the light-harvesting units, the **T2R** systems produced around twice as much hydrogen as their **T1** counterparts. Continuing irradiation for a total of 22 hours almost doubled the TON values for the **Cat1** systems, while the **Co** dyads showed no increase in produced hydrogen, meaning they had lost their activity during the first 4 hours. For all systems, the Faradaic efficiency decreased between 4 and 22 hours of irradiation (to ≈ 35 % for **Cat1** and ≈ 3 % for **Co**).

Post-operando characterization

Molecular dyads were desorbed post-operando from the NiO film in a phenylphosphonic acid methanolic solution, with the aim to quantify the amount of dyad desorbed from the NiO surface during the course of the photoelectrochemical tests as well as to identify potential structural modifications. The absorbance of the desorption solutions was measured to quantify the remaining amount of dyad still present on the surface after a 22h PEC experiment. The resulting spectra are shown in Figure 6 and Figure S9, together with the spectra recorded for the corresponding dyads desorbed from a fresh film for comparison.

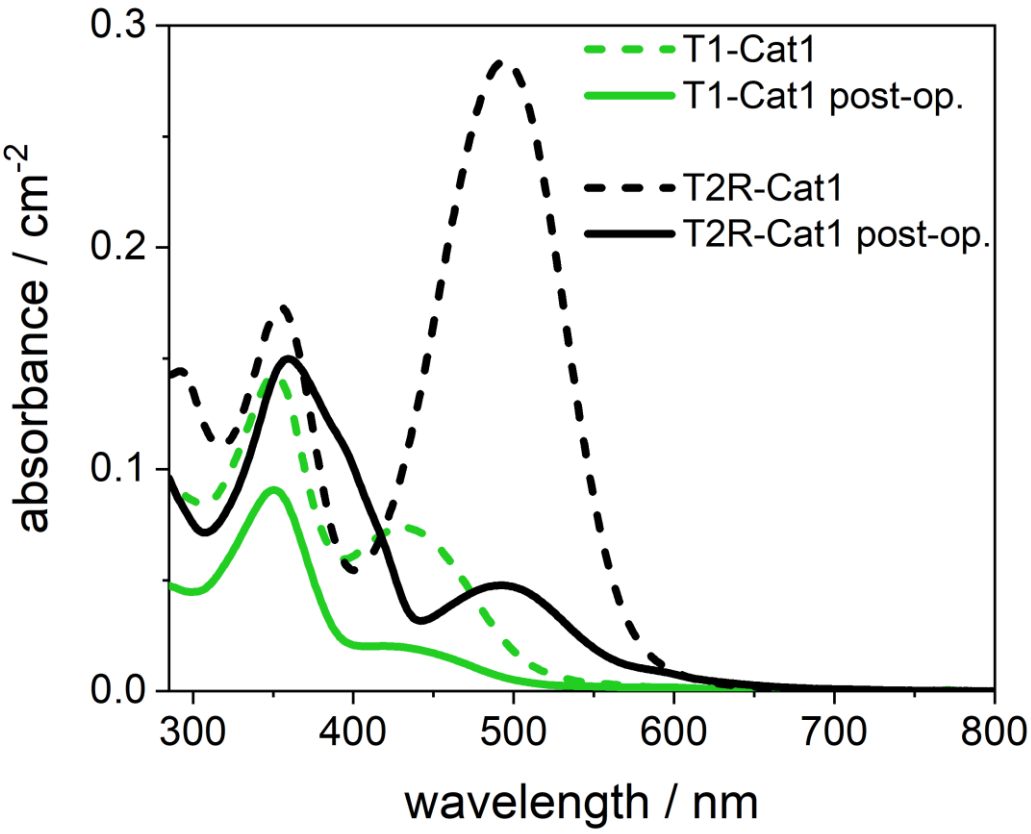

Figure 6. UV-Vis spectra of the **Cat1** dyads desorbed from fresh (dashed lines) and post-operando (after 22h of photoelectrochemical activity assessment, solid lines) NiO films in a 1 M phenylphosphonic acid solution in methanol, normalized to the surface area of the films.

The post-operando UV-Vis spectra show a particularly pronounced decrease in absorption for the ICT band at 435 and 495 nm for the **T1-** and **T2R-**based systems, respectively. We attribute the minor decrease in absorbance at the TPA band (355 nm) to a partial release of the dyads into the electrolyte solution during the PEC experiments. The decrease in absorbance at this position is less pronounced for **T2R-Cat1** in comparison to **T1-Cat1** (16 vs. 37 %), indicating a lesser degree of desorption which we ascribe to the protection against hydrolysis granted by the hydrophobic alkyl chains on the CPDT linker.[38] The strong decrease in absorbance at the ICT band, accompanied by the formation of a new band at 400 nm for **T2R-Cat1**, is likely caused by structural modification of the dye during the photoelectrochemical experiments, which expose the dye to relatively harsh conditions, *i.e.* applied reductive potential, light

irradiation and aqueous buffer. We therefore decided to investigate which of these parameters is likely at the origin of the changes in dye absorption.

For this purpose, UV-Vis absorption spectra were recorded over time in a home-made cell on NiO films sensitized with **T2R-Cat1** while varying the experimental parameters, including full operando conditions. First, spectra were recorded over one hour on a **T2R-Cat1**-sensitized NiO film with the operando potential applied in the absence of irradiation (Figure S10a); under these conditions, no spectral change was observed, apart from an initial jump in absorbance caused by the electrochromic nature of NiO.[62,63] Second, when the film was submitted to visible light irradiation in the absence of any applied potential (Figure S10b), small amplitude spectral changes were observed that might be explained by isomerization of the cyanoacrylate double bond.[64] By contrast, when the film was exposed both to visible light irradiation and to the applied potential, *i.e. operando conditions*, fast spectral changes were observed (Figure 7a), with features similar to those previously identified for the desorbed dyad in the post-operando measurements (Figure 5). A kinetic analysis revealed a biexponential decay with characteristic lifetimes of 6 and 90 min (Figure S11). In comparison, a **T2R**-sensitized NiO film displayed faster degradation kinetics, with ≈1 and 21 min characteristic lifetimes (Figure S12-13). Thus, it appears that both the applied potential and the visible light irradiation are necessary to cause the dye modification observed post-operando; in addition, this process seems to be accelerated when the catalyst is not present at the surface of the film.

To further study this process, UV-Vis spectroelectrochemical experiments were recorded on ^{tBu}**T2R** in dry 0.1 M *n*Bu_4NBF_4 acetonitrile (ACN) solution. Under these conditions, the same irreversible spectral changes were observed upon exhaustive reduction of the dye (Figure S14), thus excluding any contribution from the aqueous electrolyte in the former experiments. ^{tBu}**T1** showed an identical spectral response upon reduction, suggesting the same degradation process also takes place for this dye (Figure S14c).

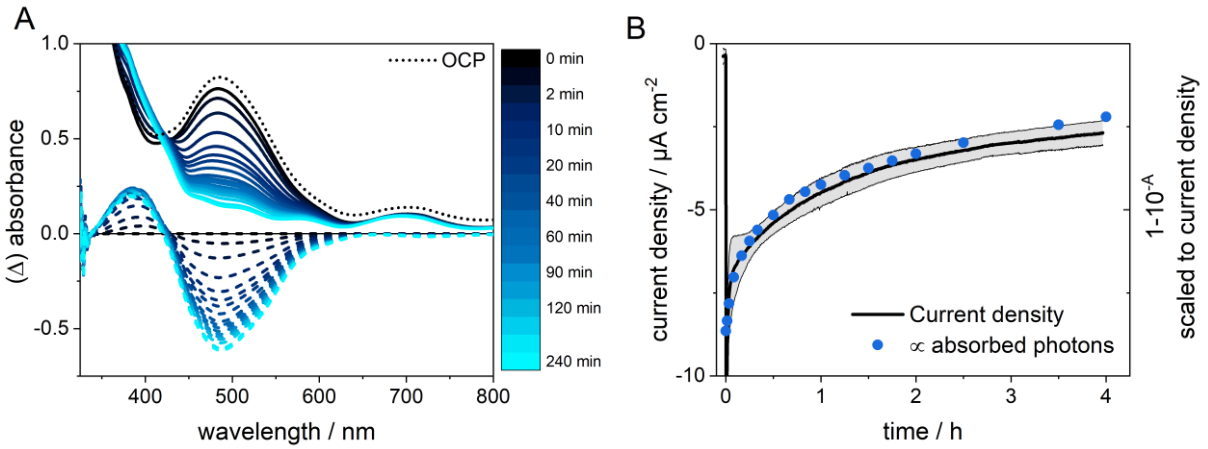

Figure 7. a) UV-Vis absorption monitoring of **T2R-Cat1**-sensitized NiO films under operando photoelectrochemical conditions: UV-Vis spectra (solid) and differential spectra (dashed) obtained by subtracting the spectrum obtained at applied potential before irradiation (0 min). b) Average current density of four different **T2R-Cat1**-sensitized NiO films plotted against $1\text{-}10^{-A}$, where A is the integrated absorbance in the visible range recorded during the operando UV-Vis measurements after subtracting the NiO background. $1\text{-}10^{-A}$ is proportional to the number of absorbed photons and was scaled to the current density at 600 s to account for the initial current spike.

To ascertain whether the modification suffered by the dye leads to the loss of the catalytic center, *e.g.* by bond cleavage, the amount of Co present at the surface of the film was determined pre- and post-operando by ICP-MS (Table S5). After respectively 4 and 22 h of PEC activity, 84 and 93 % of the initial amount of Co was lost, which correlates very well to the loss of absorbance (84 % after 4 h). Furthermore, the photocurrent recorded on **T2R-Cat1**-sensitized NiO films correlates with the number of absorbed photons (Figure 7b), which is also tied to the absorbance. These findings suggest that the same underlying process causes both the loss of Co and of the dye absorbance, as separate, independent processes would lead to a stronger loss of photocurrent compared to either the loss of absorbance or of Co loading. Assuming therefore that the correlation between the photocurrent decrease and the loss of catalytic unit holds true, the average surface concentration of intact dyads present during the first four hours of activity was estimated to be 2.0 ± 0.4 nmol·cm^{-2}, leading to a more accurate TON value of 94 ± 16 (Table S6).

Time-resolved spectroscopy and spectroelectrochemistry

Since the light-induced processes in the dye-sensitized photocathodes are crucial to charge the catalyst and thus enable catalytic proton reduction, they were investigated by time-resolved spectroscopy. In a first step, time-resolved emission was measured for all compounds grafted onto NiO and ZrO_2 films, the latter serving as a non-quenching reference (see the Supporting Information for a detailed analysis, and Figure S15, Table S7). All systems showed a complete emission quenching within the duration of the instrumental response function (FWHM = 430 ps) on NiO, which was not observed on ZrO_2. This quenching is attributed to hole injection from the excited dye into the valence band of the NiO film.[65–68]

To further investigate the sensitized NiO films, we turned to transient absorption (TA) spectroscopy. We aimed to investigate the electron transfer dynamics under conditions that are as close as possible to the operando ones, *i.e*. with the operando potential applied to the film, albeit in the absence of catalysis in order to accumulate and detect the reduced Co species, which was achieved by using dry acetonitrile as solvent. Compared to unbiased dye-sensitized NiO films, applying an external negative bias was recently shown to sharply slow down the recombination rate of reduced dye molecules with holes in the NiO film.[43,44,69] This phenomenon is attributed to the suppression of a detrimental nongeminate recombination pathway by populating the NiO intragap states upon applying a negative potential.[43] To study the influence of applied potential on the photoinduced kinetics, we performed TA-SEC experiments on NiO films sensitized either with the dyad **T2R-Cat1** or the dye **T2R** as reference. In these measurements, data was recorded at open-circuit potential (OCP), *i.e*. in the electrolyte but without any applied bias, as well as during application of two cathodic potentials to the sensitized film: first, the potential employed in the photoelectrochemical experiments (–0.74 V vs. $Fc^{+/0}$ ≙ –0.4 V vs. Ag/AgCl), sufficient to reduce the catalyst to its Co^{II} state;[17] then, a more cathodic one (–1.15 V vs. $Fc^{+/0}$) where the catalyst is reduced to the Co^{I} state. The latter measurement served as a reference since no electron transfer is thermodynamically possible to

the catalyst in the Co^{I} state (the third reduction process on the catalyst occurs at more negative potential than the dye reduction – see Figure 2). A detailed spectroscopic analysis of the fs- and ns-TA data is provided in the Supporting Information and the characteristic time constants are summarized in Table S8. Since both **T2R**- and **T2R-Cat1**-sensitized NiO films showed the same behaviour in the fs-TA-SEC experiment, they will be discussed together.

After laser pulse excitation and regardless of the potential applied to the electrode, the fs-TA spectra of **T2R-** and **T2R-Cat1**-sensitized NiO films initially show ground-state bleach (GSB) at 500 nm and excited state absorption (ESA) at > 550 nm, attributed to the vibrationally hot excited state of the dye (Figure 8, Figure S16-17).[70] This is followed by a fast recovery of GSB accompanied by a blue-shift of ESA to form a band with a maximum at 620 nm. Since the 620-nm band is characteristic of the one-electron reduced dye (Figure S18), this first process is assigned to hole injection, leading to the formation of the primary charge-separated state NiO^{+}|**T2R^{-}(-Cat1)**. Applying a three-component exponential fit to the data, a characteristic time constant of $\tau_1 < 1$ ps is obtained for this process, in line with the ultrafast hole injection observed in literature for other organic dyes grafted on NiO.[15,25,71–79]As this class of push-pull organic dyes are known to undergo a fast relaxation cascade to the relaxed ICT state on the same sub-ps time scale (Figure S17),[40,50,70,71,80–82] it seems likely that hole injection and the relaxation cascade occur simultaneously and that τ_1 therefore reflects a convolution of the two. A second process, with a characteristic time constant $\tau_2 \approx 8$ ps, can be assigned to the decay of residual excited state to the ground state since the spectral change it causes is a loss of the typical features of the **T2R** dye in the excited state. This excited state likely decays through hole injection coupled to fast charge recombination, as the latter has been previously observed on similar timescales for NiO films sensitized with organic dyes.[25,74,83]

The final spectral change is a decay of the characteristic feature of the reduced dye at 620 nm and of the remaining GSB and is thus assigned to charge recombination. This process shows a strong dependence on the applied potential: at OCP, the signal of the primary charge-separated

state completely decays within the time window of 1.6 ns, while it is very long-lived when a cathodic potential is applied to the film. This is also reflected in the time constant obtained from the fit, which increases from τ_3 = 190 ps for **T2R** and 110 ps for **T2R-Cat1** at OCP, similar to values found in literature,[15,72–77,79,83,84] to > 1 ns at –0.74 V and –1.15 V vs. $Fc^{+/0}$. Such behaviour of dye-sensitized NiO films has previously been associated with filling of intragap trap states.[43,44] These trap states are caused by Ni^{3+} defects on the NiO surface and provide a pathway for fast non-geminate charge recombination for electrons localized on the reduced dye, leading to characteristic lifetimes in the picosecond range for charge recombination.[43,66,67,72,76,85,86] Indeed, charge recombination may be so fast that no signal of the reduced dye is observed.[43,66] Application of a cathodic potential fills these trap states, thus deactivating the charge recombination channels and extending the charge-separated state lifetime. Most importantly regarding the activity for hydrogen evolution, on the timescale of the femtosecond transient absorption measurements (< 1.6 ns) there is no spectral evidence for electron transfer from the reduced dye to the catalyst in the **T2R-Cat1**-sensitized films.

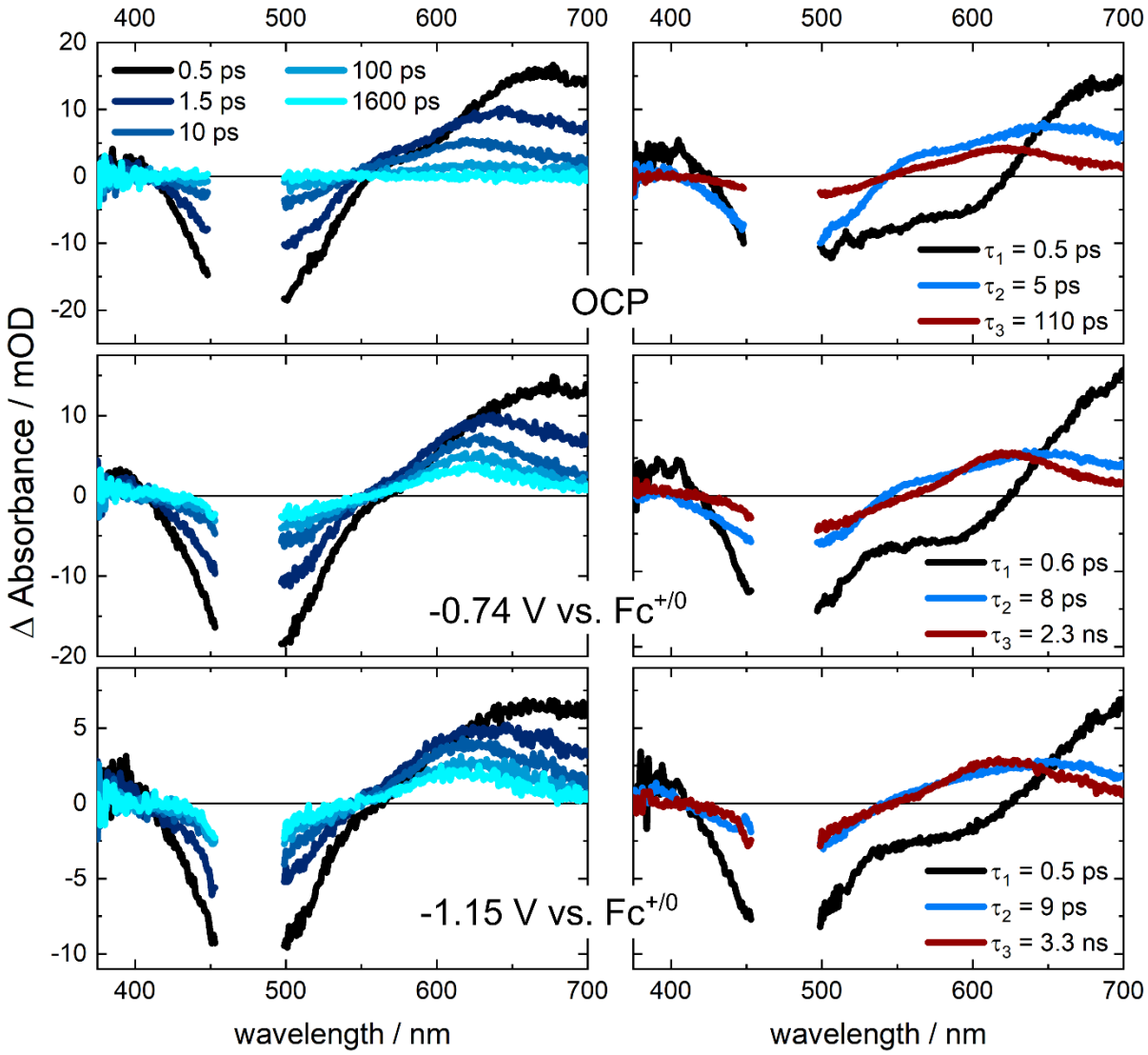

Figure 8 Left: fs-TA-SEC spectra at different pump-probe delay times after excitation at 480 nm of **T2R-Cat1**-sensitized NiO films at OCP, –0.74 V (corresponding to +0.14 V vs. RHE employed for the PEC tests) and -1.15 V vs. $Fc^{+/0}$ applied potential, using 0.1 M nBu$_4$NBF$_4$ electrolyte in ACN. Right: Decay-associated spectra obtained with a three-component exponential fit of the respective fs-TA-SEC data. τ_1 corresponds to hole injection with associated relaxation, τ_2 to a decay of residual excited state and τ_3 to charge recombination from the charge-separated state.

To accurately determine the lifetime of the primary charge-separated state and to investigate if electron transfer to the catalytic center occurs on a longer time scale, we turned to nanosecond TA-SEC experiments (which cover the time range from 20 ns to 1 ms). Kinetic traces measured at 620 and 505 nm represent the primary charge-separated state NiO^+|**T2R$^-$(-Cat1)** with the electron localized on the dye unit (Figure 9, S19). The long-lived signal decaying in a non-exponential fashion on a microsecond timescale indicates charge recombination, as observed in dye-sensitized NiO films.[13,43,44,87] For **NiO|T2R-Cat1**, the average lifetime of the primary

charge-separated state extracted from the fit at –0.74 V vs. $Fc^{+/0}$ was 7 µs, while at –1.15 V vs. $Fc^{+/0}$ it increased by more than one order of magnitude to 131 µs (27% relative decay amplitude) and > 1 ms (73% relative decay amplitude). **NiO|T2R** showed a similar trend with somewhat longer lifetimes, especially at –0.74 V vs. $Fc^{+/0}$ (τ_{ave} = 28 µs, –1.15 V vs. $Fc^{+/0}$: 184 µs (67%) and > 1 ms (33 %), Table S8).

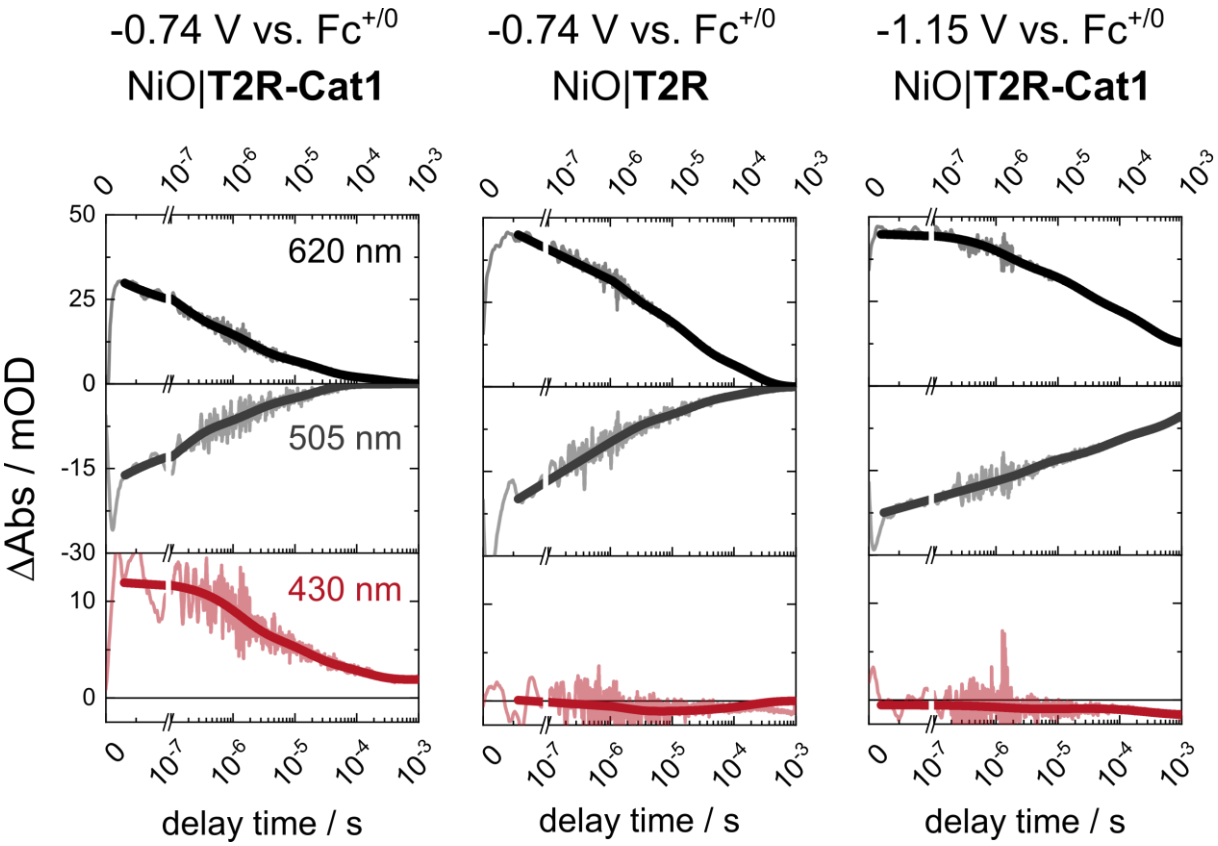

Figure 9. Kinetic traces at characteristic wavelengths obtained in ns-TASEC experiments recorded on NiO films sensitized with **T2R** and **T2R-Cat1** at applied potentials of –0.74 and –1.15 V vs. $Fc^{+/0}$, using 0.1 M nBu$_4$NBF$_4$ electrolyte in ACN. The signals at 620 and 505 nm are characteristic of the reduced state of the **T2R** dye, while the signal at 430 nm is ascribed to the Co^{I} state of the catalyst.

Within the time of the pump pulse of the ns-TA-SEC experiment (< 20 ns), a positive signal is formed at 430 nm for **T2R-Cat1** at –0.74 V vs. $Fc^{+/0}$. Measurements at several wavelengths between 400 and 460 nm reveal a positive transient absorption band with a maximum at 430 nm, characteristic wavelength of the Co^{I} state of the catalyst (Figures 10, S20-21).[33] Furthermore, this positive signal is absent when the catalytic unit is not present at the surface of the film (**T2R** at –0.74 V vs. $Fc^{+/0}$), or when it is already reduced to the Co^{I} state prior to

excitation (**T2R-Cat1** at –1.15 V vs. $Fc^{+/0}$), *i.e.* two conditions where no electron transfer is possible (Figure 9). This allowed us to unambiguously assign this spectral signature to the formation of the Co^{I} state of **Cat1** by thermally activated electron transfer from the reduced dye species.[33]

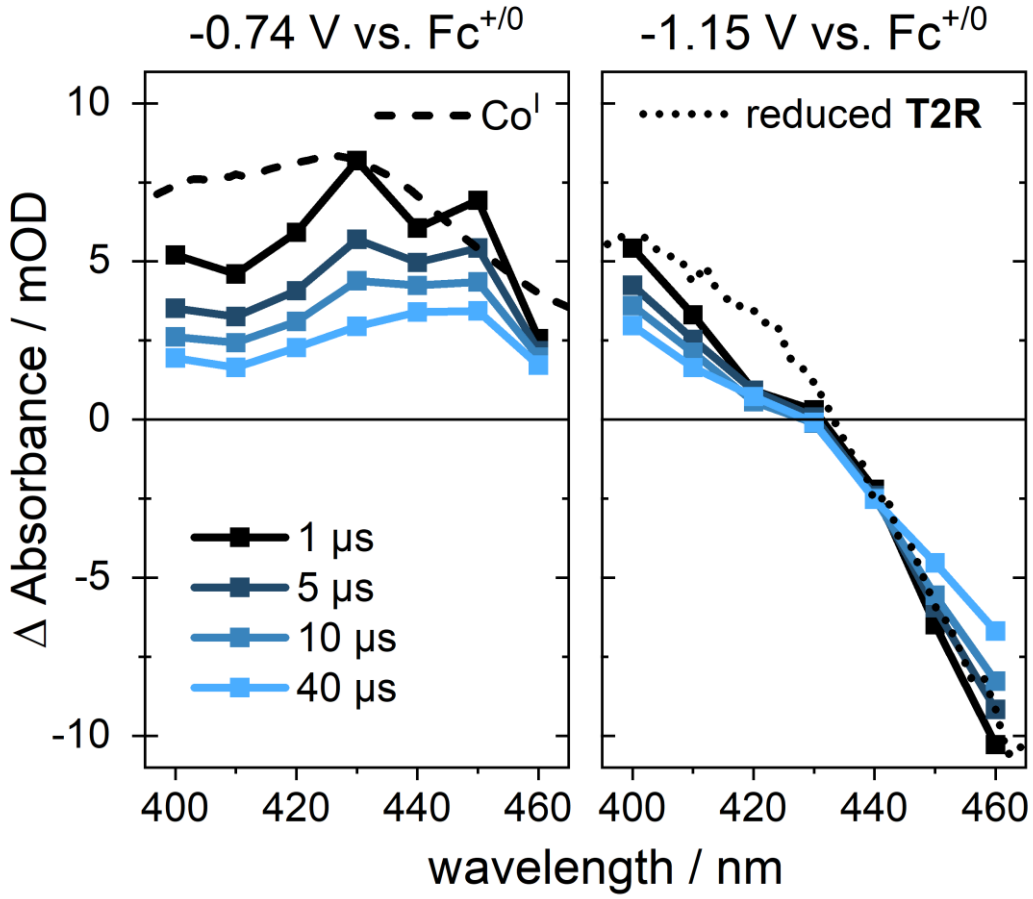

Figure 10. ns-TASEC spectra recorded on a NiO film sensitized with **T2R-Cat1** at –0.74 V and –1.15 V vs. $Fc^{+/0}$ applied potentials at different delay times together with reference spectra obtained via UV-vis SEC of the Co^{I} state (dashed) and of the one-electron reduced **T2R** in solution (dotted).

Regarding the kinetics of the electron transfer from the reduced dye to the cobalt catalyst, its absence in the fs-TA experiments combined with the maximum signal at 430 nm being present directly after the pump pulse in the ns-TA experiment puts the characteristic time constant for this process in a time window comprised between 1.6 and 20 ns. In addition, the faster decay of the signal of the reduced dye in the dyad compared to **T2R** is likely caused by an additional,

slower electron transfer process to the catalyst in the dyad. Assuming the decrease in lifetime of the reduced dye in **T2R-Cat1** in comparison to **T2R** is only due to this further process, its characteristic time constant is estimated to be 9 µs. Once formed, the Co^{I} state undergoes much slower charge recombination than the reduced dye, with average lifetimes of 30 µs (84 % relative decay amplitude) and > 1 ms (16 % relative decay amplitude).

In summary, the TA-SEC experiments revealed the following scheme (summarized in Figure 11 and S22):

(i) after light excitation, an ultrafast hole injection process leads to the generation of the primary charge-separated state NiO^{+}|**T2R**$^{-}$**-Cat1**,

(ii) the subsequent thermal electron transfer to the cobalt catalyst predominantly takes place within 20 ns, and the lifetime of the catalytically competent Co^{I} state ranges from the µs to the ms timescale,

(iii) the yield of this thermal electron transfer process is however far from unity, with a substantial amount of reduced dye still detectable at the surface of the film with an average lifetime of 7 µs.

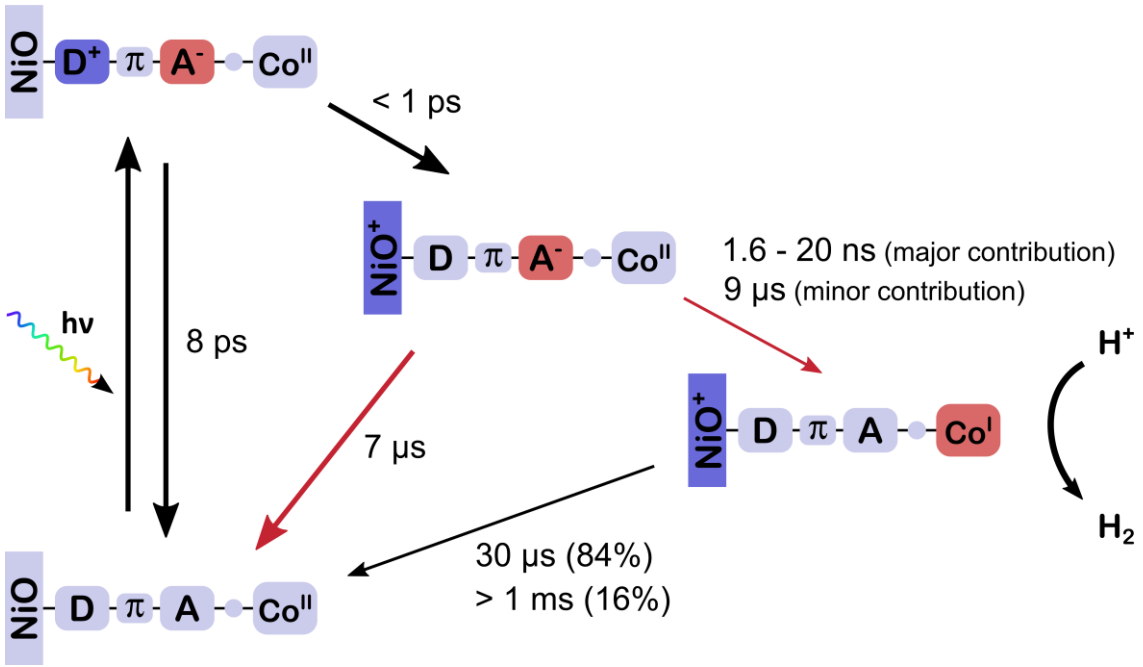

Figure 11. Scheme summarizing the light-induced processes in a **T2R-Cat1**-sensitized NiO film at –0.74 V vs. $Fc^{+/0}$ (corresponding to the +0.14 V vs. RHE potential applied during the photoelectrochemical measurements). The times indicated are inverse first order rates. Since

the charge recombination and electron transfer processes are non-exponential, the times given are averages of the inverse first order rates of a multiexponential fit (see Table S8).

Discussion

The photocathodes introduced in this study contain the tetraazamacrocyclic cobalt catalyst **Cat1** and clearly display improved performances compared to their counterparts relying on the cobalt diimine-dioxime catalyst **Co**. Although quite similar photocurrent densities were recorded (≈10 μA·cm^{-2} @ +0.14 V vs. RHE), significantly higher amounts of hydrogen were produced during the course of a 4 hours chronoamperometric measurement (up to 200 nmol·cm^{-2} for **T2R-Cat1** versus 10 nmol·cm^{-2} for **T2R-Co**), thanks to a dramatic increase in the faradaic efficiency of the process (65-70 % F.E. for **Cat1** versus 10 % F.E. for **Co**). In addition, the **Cat1** photocathodes still display some activity over 22 hours whereas the **Co** systems are fully deactivated after 4 h. TON values were calculated in order to accurately compare the efficiency of the different molecular structures while eliminating the variations in dyad loading at the surface of the NiO film. After 22 hours, 23 and 39 TONs were achieved by **T1-Cat1** and **T2R-Cat1** respectively, whereas TONs of 1 and 1.5 were recorded for **T1-Co** and **T2R-Co**, which represents a 26-fold increase. These results clearly highlight how the nature of the catalytic center is key for the photocathode performances, all the other parameters – *i.e*. dye structure, NiO film preparation, pH and nature of the electrolyte, light intensity, applied potential – being otherwise strictly identical. A straightforward comparison of these numerical values (photocurrent, amount of hydrogen produced, TON) with state of the art in the literature is difficult as these parameters vary considerably from one study to another, up to now preventing the determination of a sound structure-activity relationship. Nevertheless, the **T2R-Cat1** photocathode reported here favourably competes with the best-performing NiO ones, which are based on the cobaloxime CoHEC or the DuBois NiP catalyst.

The superior hydrogen production activity observed with **Cat1** cannot be simply rationalized thermodynamically. Indeed, both **Cat1** and **Co** dyads display a significant driving force for hole injection from the dye excited state into NiO (0.6 to 0.9 eV; see Table S1) to form the reduced dye. The reduced dye itself can subsequently reduce the catalytic center to the Co^{I} state via thermally assisted electron transfer, with very close driving forces for the two catalysts (Table S1). The clear-cut difference in the photocathode performances is rather assigned to the increased stability of **Cat1** in fully aqueous medium, which previously resulted in a 70-fold higher amount of H_2 produced under homogeneous photocatalytic conditions, compared to **Co**.[33] More generally, the robustness of polypyridinic and aminopyridinic cobalt catalysts has been recognized over the past few years[33,88–91] whereas cobaloximes are more prone to decompose under aqueous conditions of activity, via demetalation,[92] hydrolysis and/or reduction of the oxime-based ligands,[93–96] if they are not constantly and rapidly supplied with reductive equivalents.[97] The latter process might account for the low F.E. for hydrogen production of the **Co** photocathodes reported here and in previous studies from our group,[14,16,17] together with other side-reactions such as the reduction of oxygen that might diffuse in the cell during the course of the experiment.[14]

Despite having replaced **Co** by the more robust H_2-evolving catalyst **Cat1**, the overall performances of our photocathodes still need to be increased to reach a level of activity comparable to the current photoanode state of the art, with photocurrents in the $mA \cdot cm^{-2}$ range.[98] Detailed investigations on the most efficient **T2R-Cat1**-based photocathode helped us to identify two parameters currently limiting its performances:

1) Operando and post-operando characterizations revealed that the **T2R** dye structure is modified under reductive conditions, with the loss of the main part of its absorption in the visible region as a consequence. We failed to identify the exact structure of this novel derivative, although the observations that (*i*) the π-π* absorption of the triarylamine group is still present,

and (*ii*) a similar alteration is observed for **T1** and **T2R** under reductive conditions, indicate that this modification occurs on the acceptor group of the push-pull structures, *i.e*. the cyanoacrylate moiety in the case of **T2R** and the cyanoacrylamide one for **T2R-Cat1**. In addition, post-operando ICP-MS measurements indicated that an important amount of Co catalyst is lost during the first 4 hours of activity. The clear correlation found between the photocurrent decrease, the loss of absorbance and the loss of Co from the surface, strongly suggests that (*i*) the dye degradation is the main deactivation process in our system, rather than decomposition of the catalyst, and (*ii*) it involves a bond breaking, leading to the detachment of the whole catalytic center from the assembly. This is further supported by the recent observation that **Cat1** grafted on TiO_2 was stable for 10 hours under photoelectrochemical conditions similar to ours (pH 4.5 acetate buffer, 1 sun visible light irradiation),[46] rendering a catalyst-centered degradation process very unlikely. After 4 hours of activity, the dyads still intact on the surface (retained Co loading: 16 %) account for the H_2-evolving activity still detected between 4 and 22 hours. By contrast to other reported studies, where dye/catalyst desorption from the semiconductor film is the main deactivation process,[15,24,25,99] only a low amount of dyads is released in solution. The presence of the lateral alkyl chains on the CPDT bridge likely stabilizes the dyads on the NiO surface by forming a hydrophobic layer able to protect the carboxylate ester anchors from nucleophilic attack from water, as previously reported for another push-pull organic dye-based photocathode.[38] The low solubility of these dyads in aqueous medium, compared for instance to cationic ruthenium photosensitizers, might be another factor improving the stability of the sensitized NiO surface.

2) TA-SEC measurements recorded under quasi-operando conditions (same potential applied to the film as for the chronoamperometric measurements but in anhydrous acetonitrile instead of aqueous electrolyte) revealed the kinetics of the light-induced processes and provided information about the different intermediates formed at the surface of the film. First, the formation of a long-lived (> 1 ms) reduced organic dye moiety in the **T2R-Cat1** dyad was

observed due to hole injection to the NiO. The charge recombination kinetics strongly depended on the applied potential, leading to a six order of magnitude increase in the lifetime of the primary charge separated state at –0.74 V vs. $Fc^{+/0}$ with respect to OCP. While a similar behaviour was recently reported for NiO films sensitized with a push-pull organic dye[69] or ruthenium tris-diimine photosensitizers,[43,44,100] it is, to the best of our knowledge, unprecedented for a hydrogen-evolving photocathode based on a covalent dye-catalyst assembly. It must be stated that, due to similar time constants, the excited state relaxation of the dye as well as the hole injection and charge recombination processes overlapped temporally and could not be deconvoluted with the sum of exponentials analysis performed here. In the future, more advanced tools such as the recently reported stochastic kinetics simulations[101] could be applied to provide a better description of these early events. Second, thermally activated electron transfer from the reduced dye to the Co^{II} center yielding the reduced (Co^{I}) catalyst predominantly occurred on a time window of 1.6 to 20 ns, with only a small contribution taking place on longer timescales (average time constant of 9 µs). This appears to be comparable to other triazole-based dyads studied in solution, where this process has been observed on the ns-µs time scale.[53,102–105] A recent study on a Ru-Re system anchored on NiO by electropolymerization also showed electron transfer on the ns-µs scale (< 10 µs), which was attributed to electron tunnelling between the components due to the presence of an electronically insulating alkyl linker.[100] Electron transfer from a Ru dye to a Ni catalyst in a layer-by-layer assembly was determined to occur before 50 ns, either from the excited or reduced state of the dye.[23] For co-immobilised systems, charge transfer from the dye (excited or reduced state) to the catalyst has been observed in as fast as a few ps.[25,83,92,106] Direct spectroscopic observation of the reduced catalyst signature at the surface of a dye-sensitized NiO film and determination of its lifetime are however quite scarce in the literature.[25,83,100,106] The group of L. Hammarström previously reported a diiron catalyst reduced state with different lifetimes depending on the nature of its anchor to NiO: when grafted with a carboxylate

anchoring group, this reduced state was stable on the 100 µs timescale and no H_2 was produced. Employing a phosphonate anchor, the lifetime reached the ms timescale allowing for hydrogen production.[25] In our dyad, in the absence of protons, the reduced Co^I state also has a lifetime reaching the ms timescale, which can be explained by a lower driving force for charge recombination together with an increased donor-acceptor distance (e.g. Co^I to NiO^+) compared to the primary charge separated state, in which the dye is reduced. The formation of this catalytically competent species appears however to be quite inefficient; an accurate quantification of the electron transfer yield was not possible from the ns-TA-SEC experiment since the signal of the Co^I species was already built up at the beginning of the experiment, yet it was far from unity as an important amount of reduced dye remained present at the surface of the film on the µs time scale. This observation can be put in line with the presence of anodic discharging spikes when light is switched off in the chopped-light chronoamperometric measurements (Figure 4b), corresponding to the reoxidation of this accumulated reduced dye.

Taken altogether, these data highlight that neither a low light absorption efficiency nor a sluggish multielectronic catalytic process limit the dye-sensitized photocathode performances. Rather, the accumulation of photogenerated charges at the surface of the NiO film must be considered as the performance-limiting factor. Similar observations were recently made for organic semiconductor photocathodes with a perylene diimide (PDI) acceptor polymer: an upper limit for charge accumulation was determined for stable long-term operation, above which the PDI underwent irreversible change. In our case, the reduced state of the dye is not stable, which causes the loss of the catalytic unit, accompanied by a strong decrease of the light harvesting efficiency in the visible region. This process is clearly accelerated in the absence of the catalyst (**T2R** *vs.* **T2R-Cat1** photocathode) highlighting that electron transfer to the catalyst can compete with the reduced dye alteration. A fast electron transfer to the catalyst indeed reduces the lifetime of the reduced dye and thereby protects it from degradation. This charge extraction process is unfortunately not very efficient for the **T2R-Cat1** photocathode,

suggesting that only a small fraction of dyads is fully operative at the surface of the film, possibly for conformational or topological reasons. This raises questions regarding the covalent design of our dye-catalyst assemblies; indeed, the presence of a flexible methylene spacer between the acceptor side of the dye and the triazole-catalyst moiety might prevent the thermal electron transfer step, thus occurring only in very specific conformations of the assembly. Future work should clearly focus on the design of novel photocathode architectures, integrating dyes that are more robust under reductive conditions, and bridging units allowing a faster and more efficient electron supply to the catalyst.

Conclusion

In conclusion, we successfully synthesized two novel noble metal-free covalent dye-catalyst assemblies based on the robust H_2-evolving tetraazamacrocyclic cobalt catalyst **Cat1**. The performances of the resulting photocathodes were assessed under conditions strictly identical to our previously reported dyad based on the cobalt diimine-dioxime catalyst,[14,16] enabling to establish structure-activity relationships. Switching to **Cat1** was instrumental to increase both the activity and the stability of the systems, which could be further improved by the introduction of an alkyl-substituted CPDT bridge in the push-pull structure of the dye (**T2R**). The resulting **T2R-Cat1**-sensitized photocathode effectively produced hydrogen during 4 hours with 70 % Faradaic efficiency and still displays some activity after 22 hours, which ranks this construction within the best-performing H_2-evolving dye-sensitized photocathodes reported up to now[24,107,108] and opens perspectives toward an integration into a tandem photoelectrochemical cell. In order to provide meaningful insights into the factors affecting the performances of the **T2R-Cat1**-sensitized photocathode over time, we relied on a combination of operando and post-operando characterization techniques. Hence, we established that the dye structure is altered under reductive conditions. This non-exponential process, occurring on a minute to hour timescale, is correlated to the photocurrent decrease and to the loss of Co observed during the

first four hours of photoelectrochemical activity. Thus, despite significant improvements, stability is still hampered by the lack of robustness of the organic dye. In parallel, the electron transfer dynamics at the NiO interface were investigated thanks to transient absorption measurements recorded with the operando potential applied to the film. We detected the formation of the catalytically competent Co^{I} state with a lifetime of > 1 ms, sufficient to initiate catalysis.

From these results, one major bottleneck hindering photoelectrochemical performances is the low yield of the thermal electron transfer from the reduced dye to the catalyst; in addition to limiting the photocurrent density, this leads to the accumulation of charges on the acceptor part of the dye and ultimately to its degradation. This study thus provides a clear rational toward the optimization of the performances of dye-sensitized photocathodes for hydrogen production and we will focus our efforts on designing novel dyad assemblies and/or photocathode architectures achieving faster electron transfer to the catalyst. In that context, a DFT-driven approach exploiting Marcus theory to determine structures warranting higher electron transfer rates could be very valuable. Replacing NiO by other p-type semiconductors represents another track for improvement, as recently highlighted in studies by our group and others.[7,18,19] Finally, this work paves the way for the integration of robust cobalt polypyridinyl catalysts into functional photoelectrochemical devices for solar fuels production.[88,89,109]

Experimental Section.

Synthesis. All reagents were purchased from Sigma Aldrich or Strem and used as obtained unless otherwise stated. Reagent-grade solvents were used without further purification. ^{1}H NMR experiments were carried out on Bruker Avance 300 or 500 MHz spectrometers and the resulting spectra are referenced to the residual solvent peak and reported in relative to tetramethylsilane reference (δ = 0 ppm). Electrospray ionization mass spectrometric (ESI-MS)

measurements were carried out on a Thermoquest Finnigan LCQ spectrometer. Accurate mass measurements (HRMS) were recorded on a Bruker maXis mass spectrometer by the "Fédération de Recherche" ICOA/CBM (FR 2708) platform. Elemental analysis was performed on a Thermofisher Scientific “Flash 2000” by the “Plateforme d’analyse pour la chimie” (GDS 3648, Strasbourg). **^{tBu}T1**,[48] its alkyne derivative **^{tBu}T1-alkyne**,[16] **Cat1**[33] and **^{tBu}T1-Co**[16] were synthesized according to previously reported procedures. Detailed syntheses for the dye precursors, the 4-azido-2,6-diacetylpyridine building block, **^{tBu}T2R**, its alkyne derivative **^{tBu}T2R-alkyne** and **T2R-Co** are described in the Supporting Information.

General procedure for the CuAAC click coupling.[14,16] The alkyne-substituted dye (0.5 mmol) and 4-azido-2,6-diacetylpyridine (1 equiv.) were dissolved in 20 mL of degassed CH_2Cl_2. Sodium ascorbate (0.5 mmol) and $CuSO_4{\cdot}5H_2O$ (0.2 mmol) were dissolved in 10 mL of degassed H_2O and added to the reaction mixture. Degassed MeOH was added dropwise until a single phase was obtained. The reaction mixture was stirred at room temperature for 24 hours. After removal of the volatile solvents, the mixture was extracted with CH_2Cl_2, washed with brine solution, dried over Na_2SO_4 and filtered. The crude product was purified on silica gel column to yield the diacetylpyridine-functionalized dye.

*General procedure for the template synthesis of **Cat1***. The diacetylpyridine-functionalized dye (0.3 mmol) was dissolved in EtOH (2 mL) and CH_2Cl_2 (1 mL), and kept at 40 °C under argon. $CoCl_2{\cdot}6H_2O$ (1 equiv.) and water (0.4 mL) were added and the solution was stirred at 55 °C to dissolve the salt. The reaction mixture was warmed to 75°C before addition of 3,3’-diaminodipropylamine (1 equiv.) and glacial acetic acid (0.03 mL) and was then stirred at 75 °C for 5 hours under argon. After cooling down to room temperature, 0.1 mL of concentrated HCl was added and the reaction mixture was stirred at room temperature for 16 hours, then kept for 2 hours at -15 °C and centrifuged. The precipitate was washed with H_2O and EtOH before drying under vacuum to yield the dyad as a red solid.

General procedure for the tert-butyl ester groups hydrolysis prior to film sensibilisation. Hydrolysis of the tert-butyl ester groups was carried out according to our previously reported procedures,[14,16,48] by reacting the *tert*-butyl ester protected dyads (or dyes) with trifluoroacetic acid (TFA) in CH_2Cl_2 for 5 hours at room temperature.

NiO film preparation and sensitization. NiO films were prepared using a F108 precursor solution prepared by mixing 1 g of $NiCl_2$, 1 g of F108 triblock copolymer in a mixture of ethanol (15 mL) and Milli-Q water (6 mL), according to our previously reported procedures.[14,16] The mixture was sonicated for 6 h, centrifuged and passed through a 45 µm pore size polyethersulfone syringe filter. FTO-coated glass substrates (Solems TEC 7, sheet resistance 7Ω.□) for the hydrogen production experiments or round ITO-coated glass substrates (Solems ITO SOL 30, 1 mm thickness) for the operando UV-Vis experiments and transient absorption measurements were cleaned by sonication in isopropanol, distilled water and ethanol for 10 min each, followed by ozone cleaning for 15 min. The F108 precursor solution was then spin-coated on the substrates (5000 rpm, 60 s) followed by sintering in an oven in air (30 min ramp to 450 °C, 30 min at 450 °C). Spin-coating and sintering was repeated for a total of four layers. The film thickness was measured by scanning electron microscopy (SEM) with a scanning electron microscope Zeiss Ultra 55 operating at 4 kV.

NiO electrodes were soaked in methanolic solutions (0.2 mM) of the different dyes and dyads (acidic form) at room temperature for 24 h under orbital stirring. For the TCSPC measurements, sensitizing solutions with 10 mM chenodeoxycholic acid (CDCA) added were used for sensitization. After sensitization, films were then rinsed with methanol and dried with pressured air. After sensitization, NiO films were cut in half. One half of the sample was used to determine grafting densities pre-operando while the other half was used for photoelectrochemical experiments and afterwards desorbed to determine grafting densities and possible degradation post-operando.

Dyad loading quantification. Sensitized NiO films were soaked in 1M methanolic phenylphosphonic acid solution for 3 hours to desorb grafted compounds. Afterwards, UV-Vis spectra of the desorption solutions were then measured and dyad (or dye) loading was determined using the molar extinction coefficient at the $\pi-\pi*$ band (Figure S3) and the film surface areas. Cobalt quantification was performed by inductively coupled plasma mass spectrometry (ICP-MS) using an iCAP RQ quadrupole mass instrument (Thermo Fisher Scientific GmbH, Germany). The samples were prepared by soaking each film in 1 mL of aq. HNO_3 (65% w/v) for 1 min, rinsing with 1 mL Milli-Q water, hydrolyzing again with 1 mL of HNO_3, rinsing with 1 mL H_2O, then 2.5 mL H_2O. The resulting solution (6.5 mL at 20% w/v HNO_3) was diluted 20 times to yield a solution at 1% w/v HNO_3, which was used for the measurement.

Steady-state spectroscopy. Steady-state absorption spectra were recorded on an Agilent Cary 60 or a Jasco V780 spectrophotometer in 1 cm cuvettes. All solvents used for spectroscopy were of spectroscopic grade.

Time-correlated single photon counting (TCSPC) measurements. The emission decay profiles were measured by time-correlated single photon counting (TCSPC) in a time window of 20 ns. After excitation of the sample with the frequency-doubled output of a Ti-sapphire laser (Tsunami, Newport Spectra-Physics GmbH) at λ_{ex} = 365 nm at a pulse-to-pulse repetition rate of 400 kHz after passing a pulse selector (model 3980, Newport Spectra-Physics GmbH), the luminescence of the sample was collected in a 90°-arrangement and detected using a Becker & Hickl PMC-100-4 photon-counting module. The lifetime values were obtained from mono- or bi-exponential fits convoluted with the instrument response function (IRF). Sample solutions were prepared to yield an optical density of 0.05-0.1 at the excitation wavelength in a 1.0 cm quartz cuvette using air-equilibrated, spectroscopic grade solvents.

Electrochemical and photoelectrochemical experiments. Electrochemical and photoelectrochemical experiments were recorded using either a BioLogic VSP 300, BioLogic SP 50 or Ivium CompactStat potentiostat. A three-electrode setup was used for all experiments. For electrochemical experiments, Merck SeccoSolv® dry DMF was used as solvent and the tetrabutylammonium tetrafluoroborate was recrystallized from ethanol/water prior to use. The working electrode was a glassy carbon disk electrode, the auxiliary electrode a Pt wire and the reference electrode a miniature leakless Ag/AgCl electrode (EDAQ). The supporting electrolyte was 0.1 M $TBABF_4$ in dry DMF, degassed by passing argon through the solution for 20 min before measuring. During the measurements, the argon flow was removed from the solution but left in the headspace of the cell. The scan rate during cyclic voltammetry was 50 $mV \cdot s^{-1}$ and the sample concentration was 1 mM. The potential of the reference electrode was calibrated after each measurement by adding ferrocene as a reference to the solution and recording the potential of the $Fc^{+/0}$ couple.

The photoelectrochemical measurements were carried out in a home-made three-electrode cell with a sensitized NiO film as working electrode, a titanium wire as auxiliary electrode and a Ag/AgCl reference electrode made of a Ag/AgCl wire dipped into a 3 M aqueous KCl solution, separated from the electrolyte by a Vycor® frit. The auxiliary electrode was separated from the main compartment of the cell by a Vycor® frit. Irradiation was performed using a Newport 300 W ozone-free Xe lamp at either 280 or 130 W equipped with a water-filled Spectra-Physics 6123NS liquid filter to eliminate infrared radiation ($\lambda > 800$ nm) and a 400 nm longpass filter (Spectra-Physics 59472). The power density was measured using a Newport PM1918-R power-meter and adjusted to 65 $mW \cdot cm^{-2}$ (equivalent to one sun irradiation) using appropriate neutral density filters. The aqueous supporting electrolyte was either 0.1 M 2-(N-morpholino)ethanesulfonic acid (MES)/0.1 M NaCl buffer at pH 5.5 or 0.12 M Britton-Robinson buffer at pH 4.5, 5.5 or 7.0, as also stated in the respective data description. The electrolyte solution was degassed with nitrogen for 30 minutes prior to use. The amount of

hydrogen evolved produced during the long-term chronoamperometric measurements was measured in the headspace by sampling aliquots in a Perkin Elmer Clarus 580 gas chromatograph equipped with a molecular sieve 5 Å column (30 m – 0.53 mm) and a TCD detector. Additionally, the amount of hydrogen dissolved in solution was determined by a Unisense H_2 microsensor in a needle. The zero value for the microsensor was measured in the assembled cell prior to irradiation.Potentials are given as converted to potentials vs. reversible hydrogen electrode (RHE) using the formula:

$$E_{RHE} = E_{Ag/AgCl} + 0.425\,V - E_{Fe(III)/Fe(II)} + 0.059 * pH$$

where 0.425 V is the potential of the potassium ferrocyanide Fe(III)/Fe(II) couple vs. NHE at 0.1M potassium phosphate buffer at pH 7[110] and $E_{Fe(III)/Fe(II)}$ is the potential of the potassium ferrocyanide $Fe^{III/II}$ couple measured vs. the Ag/AgCl reference electrode.

For the photoelectrochemical degradation experiment, a home-made spectroelectrochemistry cell specifically designed for measurements on transparent semiconductor films was used with dye-sensitized NiO films on ITO/glass substrate (Solems, ITO SOL 30, 1 mm thickness) as working electrode, Pt wire as auxiliary electrode and a miniature leakless Ag/AgCl (EDAQ) as reference electrode. The supporting electrolyte was 0.1 M 2-(*N*-morpholino)ethanesulfonic acid (MES)/0.1 M NaCl buffer at pH 5.5. The solution was degassed for 20 minutes prior to measuring. At an applied potential of –0.35 V vs. Ag/AgCl (0.21 V vs. RHE), the film was irradiated as in the photoelectrochemical experiments and UV-Vis spectra were recorded in intervals.

Transient absorption spectroelectrochemistry (TA-SEC) measurements. The setup for femtosecond transient absorption measurements has been previously described.[111] An amplified Ti:Sapphire laser (Legend, Coherent Inc) produced the 800 nm fundamental beam which was split into two beams. One of the beams was used to pump an optical-parametric amplifier

(TOPAS-C), whose output was spectrally centered at 480 nm and used as pump pulses for the pump-probe experiments. The pump pulses were typically set to 0.4 μJ per pulse, which was lowered to 0.2 μJ per pulse for measurements at –1.15 V vs. $Fc^{+/0}$ to avoid photodegradation. To achieve the pump-probe delay of 2 ns, the pump beam was directed over a delay line. The supercontinuum used as probe pulse was generated by passing the second beam of the fundamental 800 nm through a CaF_2 window, with probe intensities falling into the range of hundred nJ. The probe light was split into two beams, one of which was focussed through the sample, while the other served as reference. A 488 nm notch filter was placed between sample and detector to remove scattered pump light. The probe and reference beams were detected by a double-stripe diode array and converted into differential absorption signals using a commercially available detection system (Pascher Instruments AB, Sweden). The recorded data was corrected for the chirp and globally fitted using a sum of three exponential. During the fitting, the pulse overlap region of ± 200 fs was excluded to avoid contributions from coherent artifacts.[112]

The setup for ns transient absorption measurements was previously described:[113] The pump pulse was generated by a Continuum Surelite OPO Plus (pumped by a Nd:YAG laser, ≈20 ns pulse duration, 10 Hz repetition rate). The probe light was generated by a 75 W Xenon arc lamp and focussed through the sample and detected by a Hamamatsu R928 photomultiplier. The signal was amplified and processed by a commercially available detection system (Pascher Instruments AB, Sweden). The pump pulse energy was set to 0.13 mJ. To remove pump scatter, a 475 nm short pass and a 500 nm long pass edge filters were used for short and long wavelengths, respectively.

TA-SEC experiments were performed using a home-built spectroelectrochemical cell, designed to work in a three-electrode setup under inert conditions and to optimize time resolution in the fs measurements, with a minimized path length (ca. 4 mm). The sensitized NiO film was used as the working electrode, a miniature leakless Ag/AgCl electrode (EDAQ) as reference

electrode and a Pt wire as auxiliary electrode. The cell was assembled in a glove box and filled with 0.1 M $TBABF_4$ in ACN. Transient absorption measurements were performed at open circuit potential and different applied potentials on the same film, moving the film in the plane periodically to prevent photodegradation. Prior to each experiment, the reference electrode was calibrated using ferrocene.

AUTHOR INFORMATION

Corresponding Author

* Benjamin Dietzek; E-mail: benjamin.dietzek@leibniz-ipht.de
* Murielle Chavarot-Kerlidou; E-mail: murielle.chavarot-kerlidou@cea.fr

Present Addresses

†Present address: Aix Marseille Univ, CNRS, Centrale Marseille, iSm2, Marseille, France.

Author Contributions

The manuscript was written through contributions of all authors. All authors have given approval to the final version of the manuscript.

Funding Sources

This work was supported by the European Commission's Seventh Framework Program (FP7/2007-2013) under grant agreement n° 306398 (FP7-IDEAS-ERC, Project PhotocatH_2ode), the French National Research Agency in the framework of the "Investissements d'avenir" program (ANR-15-IDEX-02, Labex ARCANE and CBH-EURGS, ANR-17-EURE-0003) and the Franco-German University.

ASSOCIATED CONTENT

Supporting Information. The following files are available free of charge. Detailed synthetic procedures and additional spectroscopic and photoelectrochemical data (PDF).

ACKNOWLEDGMENT

Quentin Vacher, Tatiana Straistari and Adina Morozan are acknowledged for their help in the synthesis and purification of the compounds and for the SEM measurements. Jacques Pecaut (CEA/DRF/IRIG/DIESE/SyMMES) and Pierre-Alain Bayle (CEA/DRF/IRIG/DEPHY/MEM) are acknowledged for the ESI-MS and the 500 MHz NMR measurements, respectively. Stéphane Ravanel from CEA/DRF/IRIG/DBSCI/PCV is acknowledged for the ICP-MS analysis. This work was supported by the European Commission's Seventh Framework Program (FP7/2007-2013) under grant agreement n° 306398 (FP7-IDEAS-ERC, Project PhotocatH_2ode) and the French National Research Agency in the framework of the "Investissements d'avenir" program (ANR-15-IDEX-02, Labex ARCANE and CBH-EURGS, ANR-17-EURE-0003). S.B. wants to thank the Franco-German University for the cotutelle thesis funding support. We want to thank the workshop of the IPHT Jena for their help in building the spectroscopy cell.

REFERENCES

(1) Nocera, D. G. Solar Fuels and Solar Chemicals Industry. *Accounts of Chemical Research* **2017**, *50* (3), 616–619. https://doi.org/10.1021/acs.accounts.6b00615.

(2) Zhang, B.; Sun, L. Artificial Photosynthesis: Opportunities and Challenges of Molecular Catalysts. *Chemical Society Reviews* **2019**, *48* (7), 2216–2264. https://doi.org/10.1039/C8CS00897C.

(3) House, R. L.; Iha, N. Y. M.; Coppo, R. L.; Alibabaei, L.; Sherman, B. D.; Kang, P.; Brennaman, M. K.; Hoertz, P. G.; Meyer, T. J. Artificial Photosynthesis: Where Are We Now? Where Can We Go? *Journal of Photochemistry and Photobiology C: Photochemistry Reviews* **2015**, *25*, 32–45. https://doi.org/10.1016/j.jphotochemrev.2015.08.002.

(4) Berardi, S.; Drouet, S.; Francàs, L.; Gimbert-Suriñach, C.; Guttentag, M.; Richmond, C.; Stoll, T.; Llobet, A. Molecular Artificial Photosynthesis. *Chem. Soc. Rev.* **2014**, *43* (22), 7501–7519. https://doi.org/10.1039/C3CS60405E.

(5) Brennaman, M. K.; Dillon, R. J.; Alibabaei, L.; Gish, M. K.; Dares, C. J.; Ashford, D. L.; House, R. L.; Meyer, G. J.; Papanikolas, J. M.; Meyer, T. J. Finding the Way to Solar Fuels with Dye-Sensitized Photoelectrosynthesis Cells. *Journal of the American Chemical Society* **2016**, *138* (40), 13085–13102. https://doi.org/10.1021/jacs.6b06466.

(6) Yu, Z.; Li, F.; Sun, L. Recent Advances in Dye-Sensitized Photoelectrochemical Cells for Solar Hydrogen Production Based on Molecular Components. *Energy Environ. Sci.* **2015**, *8* (3), 760–775. https://doi.org/10.1039/C4EE03565H.

(7) Windle, C. D.; Kumagai, H.; Higashi, M.; Brisse, R.; Bold, S.; Jousselme, B.; Chavarot-Kerlidou, M.; Maeda, K.; Abe, R.; Ishitani, O.; Artero, V. Earth-Abundant Molecular Z-Scheme Photoelectrochemical Cell for Overall Water-Splitting. *Journal of the American Chemical Society* **2019**, *141* (24), 9593–9602. https://doi.org/10.1021/jacs.9b02521.

(8) Fan, K.; Li, F.; Wang, L.; Daniel, Q.; Gabrielsson, E.; Sun, L. Pt-Free Tandem Molecular Photoelectrochemical Cells for Water Splitting Driven by Visible Light. *Phys. Chem. Chem. Phys.* **2014**, *16* (46), 25234–25240. https://doi.org/10.1039/C4CP04489D.

(9) Li, F.; Fan, K.; Xu, B.; Gabrielsson, E.; Daniel, Q.; Li, L.; Sun, L. Organic Dye-Sensitized Tandem Photoelectrochemical Cell for Light Driven Total Water Splitting. *Journal of the American Chemical Society* **2015**, *137* (28), 9153–9159. https://doi.org/10.1021/jacs.5b04856.

(10) Ji, Z.; He, M.; Huang, Z.; Ozkan, U.; Wu, Y. Photostable P-Type Dye-Sensitized Photoelectrochemical Cells for Water Reduction. *Journal of the American Chemical Society* **2013**, *135* (32), 11696–11699. https://doi.org/10.1021/ja404525e.

(11) Li, L.; Duan, L.; Wen, F.; Li, C.; Wang, M.; Hagfeldt, A.; Sun, L. Visible Light Driven Hydrogen Production from a Photo-Active Cathode Based on a Molecular Catalyst and Organic Dye-Sensitized p-Type Nanostructured NiO. *Chemical Communications* **2012**, *48* (7), 988–990. https://doi.org/10.1039/C2CC16101J.

(12) Meng, P.; Wang, M.; Yang, Y.; Zhang, S.; Sun, L. CdSe Quantum Dots/Molecular Cobalt Catalyst Co-Grafted Open Porous NiO Film as a Photocathode for Visible Light Driven H2 Evolution from Neutral Water. *Journal of Materials Chemistry A* **2015**, *3* (37), 18852–18859. https://doi.org/10.1039/C5TA06255A.

(13) Kamire, R. J.; Majewski, M. B.; Hoffeditz, W. L.; Phelan, B. T.; Farha, O. K.; Hupp, J. T.; Wasielewski, M. R. Photodriven Hydrogen Evolution by Molecular Catalysts Using Al2O3 -Protected Perylene-3,4-Dicarboximide on NiO Electrodes. *Chemical Science* **2017**, *8* (1), 541–549. https://doi.org/10.1039/C6SC02477G.

(14) Windle, C. D.; Massin, J.; Chavarot-Kerlidou, M.; Artero, V. A Protocol for Quantifying Hydrogen Evolution by Dye-Sensitized Molecular Photocathodes and Its Implementation for Evaluating a New Covalent Architecture Based on an Optimized Dye-Catalyst Dyad. *Dalton Transactions* **2018**, *47* (31), 10509–10516. https://doi.org/10.1039/C8DT01210E.

(15) Pati, P. B.; Zhang, L.; Philippe, B.; Fernández-Terán, R.; Ahmadi, S.; Tian, L.; Rensmo, H.; Hammarström, L.; Tian, H. Insights into the Mechanism of a Covalently Linked Organic Dye–Cobaloxime Catalyst System for Dye-Sensitized Solar Fuel Devices. *ChemSusChem* **2017**, *10* (11), 2480–2495. https://doi.org/10.1002/cssc.201700285.

(16) Kaeffer, N.; Massin, J.; Lebrun, C.; Renault, O.; Chavarot-Kerlidou, M.; Artero, V. Covalent Design for Dye-Sensitized H2 -Evolving Photocathodes Based on a Cobalt Diimine–Dioxime

Catalyst. *Journal of the American Chemical Society* **2016**, *138* (38), 12308–12311. https://doi.org/10.1021/jacs.6b05865.

(17) Kaeffer, N.; Windle, C. D.; Brisse, R.; Gablin, C.; Leonard, D.; Jousselme, B.; Chavarot-Kerlidou, M.; Artero, V. Insights into the Mechanism and Aging of a Noble-Metal Free H2 -Evolving Dye-Sensitized Photocathode. *Chemical Science* **2018**, *9* (32), 6721–6738. https://doi.org/10.1039/C8SC00899J.

(18) Li, F.; Xu, R.; Nie, C.; Wu, X.; Zhang, P.; Duan, L.; Sun, L. Dye-Sensitized LaFeO3 Photocathode for Solar-Driven H2 Generation. *Chemical Communications* **2019**, *55* (86), 12940–12943. https://doi.org/10.1039/C9CC06781G.

(19) Creissen, C. E.; Warnan, J.; Antón-García, D.; Farré, Y.; Odobel, F.; Reisner, E. Inverse Opal CuCrO2 Photocathodes for H2 Production Using Organic Dyes and a Molecular Ni Catalyst. *ACS Catalysis* **2019**, *9* (10), 9530–9538. https://doi.org/10.1021/acscatal.9b02984.

(20) Wang, D.; Sheridan, M. v; Shan, B.; Farnum, B. H.; Marquard, S. L.; Sherman, B. D.; Eberhart, M. S.; Nayak, A.; Dares, C. J.; Das, A. K.; Bullock, R. M.; Meyer, T. J. Layer-by-Layer Molecular Assemblies for Dye-Sensitized Photoelectrosynthesis Cells Prepared by Atomic Layer Deposition. *Journal of the American Chemical Society* **2017**, *139* (41), 14518–14525. https://doi.org/10.1021/jacs.7b07216.

(21) Gross, M. A.; Creissen, C. E.; Orchard, K. L.; Reisner, E. Photoelectrochemical Hydrogen Production in Water Using a Layer-by-Layer Assembly of a Ru Dye and Ni Catalyst on NiO. *Chemical Science* **2016**, *7* (8), 5537–5546. https://doi.org/10.1039/c6sc00715e.

(22) Shan, B.; Sherman, B. D.; Klug, C. M.; Nayak, A.; Marquard, S. L.; Liu, Q.; Bullock, R. M.; Meyer, T. J. Modulating Hole Transport in Multilayered Photocathodes with Derivatized P-Type Nickel Oxide and Molecular Assemblies for Solar-Driven Water Splitting. *The Journal of Physical Chemistry Letters* **2017**, *8* (18), 4374–4379. https://doi.org/10.1021/acs.jpclett.7b01911.

(23) Shan, B.; Das, A. K.; Marquard, S.; Farnum, B. H.; Wang, D.; Bullock, R. M.; Meyer, T. J. Photogeneration of Hydrogen from Water by a Robust Dye-Sensitized Photocathode. *Energy & Environmental Science* **2016**, *9* (12), 3693–3697. https://doi.org/10.1039/C6EE02903E.

(24) Creissen, C. E.; Warnan, J.; Reisner, E. Solar H2 Generation in Water with a CuCrO2 Photocathode Modified with an Organic Dye and Molecular Ni Catalyst. *Chemical Science* **2018**, *9* (6), 1439–1447. https://doi.org/10.1039/C7SC04476C.

(25) Antila, L. J.; Ghamgosar, P.; Maji, S.; Tian, H.; Ott, S.; Hammarström, L. Dynamics and Photochemical H2 Evolution of Dye–NiO Photocathodes with a Biomimetic FeFe-Catalyst. *ACS Energy Letters* **2016**, *1* (6), 1106–1111. https://doi.org/10.1021/acsenergylett.6b00506.

(26) Lyu, S.; Massin, J.; Pavone, M.; Muñoz-García, A. B.; Labrugère, C.; Toupance, T.; Chavarot-Kerlidou, M.; Artero, V.; Olivier, C. H2 -Evolving Dye-Sensitized Photocathode Based on a Ruthenium–Diacetylide/Cobaloxime Supramolecular Assembly. *ACS Applied Energy Materials* **2019**, *2* (7), 4971–4980. https://doi.org/10.1021/acsaem.9b00652.

(27) Shan, B.; Brennaman, M. K.; Troian-Gautier, L.; Liu, Y.; Nayak, A.; Klug, C. M.; Li, T. T.; Bullock, R. M.; Meyer, T. J. A Silicon-Based Heterojunction Integrated with a Molecular Excited State in a Water-Splitting Tandem Cell. *Journal of the American Chemical Society* **2019**, *141* (26), 10390–10398. https://doi.org/10.1021/jacs.9b04238.

(28) Nie, C.; Ni, W.; Gong, L.; Jiang, J.; Wang, J.; Wang, M. Charge Transfer Dynamics and Catalytic Performance of a Covalently Linked Hybrid Assembly Comprising a Functionalized Cobalt Tetraazamacrocyclic Catalyst and CuInS2/ZnS Quantum Dots for Photochemical Hydrogen Production. *Journal of Materials Chemistry A* **2019**, *7* (48), 27432–27440. https://doi.org/10.1039/C9TA10479H.

(29) Grau, S.; Schilling, M.; Moonshiram, D.; Benet-Buchholz, J.; Luber, S.; Llobet, A.; Gimbert-Suriñach, C. Electrochemically and Photochemically Induced Hydrogen Evolution Catalysis with Cobalt Tetraazamacrocycles Occurs Through Different Pathways. *ChemSusChem* **2020**, *13* (10), 2745–2752. https://doi.org/10.1002/cssc.202000283.

(30) Leung, C.; Chen, Y.; Yu, H.; Yiu, S.; Ko, C.; Lau, T.-C. Electro- and Photocatalytic Hydrogen Generation in Acetonitrile and Aqueous Solutions by a Cobalt Macrocyclic Schiff-Base Complex. *International Journal of Hydrogen Energy* **2011**, *36* (18), 11640–11645. https://doi.org/10.1016/j.ijhydene.2011.06.062.

(31) Gueret, R.; Poulard, L.; Oshinowo, M.; Chauvin, J.; Dahmane, M.; Dupeyre, G.; Lainé, P. P.; Fortage, J.; Collomb, M.-N. Challenging the [Ru(Bpy)3]2+ Photosensitizer with a Triazatriangulenium Robust Organic Dye for Visible-Light-Driven Hydrogen Production in Water. *ACS Catalysis* **2018**, *8* (5), 3792–3802. https://doi.org/10.1021/acscatal.7b04000.

(32) Sandroni, M.; Gueret, R.; Wegner, K. D.; Reiss, P.; Fortage, J.; Aldakov, D.; Collomb, M.-N. Cadmium-Free CuInS2/ZnS Quantum Dots as Efficient and Robust Photosensitizers in Combination with a Molecular Catalyst for Visible Light-Driven H2 Production in Water. *Energy & Environmental Science* **2018**, *11* (7), 1752–1761. https://doi.org/10.1039/C8EE00120K.

(33) Varma, S.; Castillo, C. E.; Stoll, T.; Fortage, J.; Blackman, A. G.; Molton, F.; Deronzier, A.; Collomb, M.-N. Efficient Photocatalytic Hydrogen Production in Water Using a Cobalt(III) Tetraaza-Macrocyclic Catalyst: Electrochemical Generation of the Low-Valent Co(I) Species and Its Reactivity toward Proton Reduction. *Physical Chemistry Chemical Physics* **2013**, *15* (40), 17544. https://doi.org/10.1039/c3cp52641k.

(34) Gimbert-Suriñach, C.; Albero, J.; Stoll, T.; Fortage, J.; Collomb, M.-N.; Deronzier, A.; Palomares, E.; Llobet, A. Efficient and Limiting Reactions in Aqueous Light-Induced Hydrogen Evolution Systems Using Molecular Catalysts and Quantum Dots. *Journal of the American Chemical Society* **2014**, *136* (21), 7655–7661. https://doi.org/10.1021/ja501489h.

(35) Roy, S.; Bacchi, M.; Berggren, G.; Artero, V. A Systematic Comparative Study of Hydrogen-Evolving Molecular Catalysts in Aqueous Solutions. *ChemSusChem* **2015**, *8* (21), 3632–3638. https://doi.org/10.1002/cssc.201501002.

(36) Yen, Y.-S.; Chen, W.-T.; Hsu, C.-Y.; Chou, H.-H.; Lin, J. T.; Yeh, M.-C. P. Arylamine-Based Dyes for p-Type Dye-Sensitized Solar Cells. *Organic Letters* **2011**, *13* (18), 4930–4933. https://doi.org/10.1021/ol202014x.

(37) Li, R.; Liu, J.; Cai, N.; Zhang, M.; Wang, P. Synchronously Reduced Surface States, Charge Recombination, and Light Absorption Length for High-Performance Organic Dye-Sensitized Solar Cells. *Journal of Physical Chemistry B* **2010**, *114* (13), 4461–4464. https://doi.org/10.1021/jp101222s.

(38) Click, K. A.; Beauchamp, D. R.; Huang, Z.; Chen, W.; Wu, Y. Membrane-Inspired Acidically Stable Dye-Sensitized Photocathode for Solar Fuel Production. *Journal of the American Chemical Society* **2016**, *138* (4), 1174–1179. https://doi.org/10.1021/jacs.5b07723.

(39) Yu, Y.; Click, K. A.; Chien, S.-C.; Sun, J.; Curtze, A.; Lin, L.-C.; Wu, Y. Decoupling PH Dependence of Flat Band Potential in Aqueous Dye-Sensitized Electrodes. *The Journal of Physical Chemistry C* **2019**, *123* (14), 8681–8687. https://doi.org/10.1021/acs.jpcc.9b00710.

(40) Bold, S.; Zedler, L.; Zhang, Y.; Massin, J.; Artero, V.; Chavarot-Kerlidou, M.; Dietzek, B. Electron Transfer in a Covalent Dye–Cobalt Catalyst Assembly – a Transient Absorption Spectroelectrochemistry Perspective. *Chemical Communications* **2018**, *54* (75), 10594–10597. https://doi.org/10.1039/C8CC05556D.

(41) Zedler, L.; Mengele, A. K.; Ziems, K. M.; Zhang, Y.; Wächtler, M.; Gräfe, S.; Pascher, T.; Rau, S.; Kupfer, S.; Dietzek, B. Unraveling the Light-Activated Reaction Mechanism in a Catalytically Competent Key Intermediate of a Multifunctional Molecular Catalyst for Artificial Photosynthesis. *Angewandte Chemie International Edition* **2019**, *58* (37), 13140–13148. https://doi.org/10.1002/anie.201907247.

(42) Zhang, Y.; Zedler, L.; Karnahl, M.; Dietzek, B. Excited-State Dynamics of Heteroleptic Copper(I) Photosensitizers and Their Electrochemically Reduced Forms Containing a Dipyridophenazine Moiety – a Spectroelectrochemical Transient Absorption Study. *Physical Chemistry Chemical Physics* **2019**, *21* (20), 10716–10725. https://doi.org/10.1039/C9CP00412B.

(43) Dillon, R. J.; Alibabaei, L.; Meyer, T. J.; Papanikolas, J. M. Enabling Efficient Creation of Long-Lived Charge-Separation on Dye-Sensitized NiO Photocathodes. *ACS Applied Materials & Interfaces* **2017**, *9* (32), 26786–26796. https://doi.org/10.1021/acsami.7b05856.

(44) D'Amario, L.; Antila, L. J.; Pettersson Rimgard, B.; Boschloo, G.; Hammarström, L. Kinetic Evidence of Two Pathways for Charge Recombination in NiO-Based Dye-Sensitized Solar Cells. *The Journal of Physical Chemistry Letters* **2015**, *6* (5), 779–783. https://doi.org/10.1021/acs.jpclett.5b00048.

(45) McCrory, C. C. L.; Uyeda, C.; Peters, J. C. Electrocatalytic Hydrogen Evolution in Acidic Water with Molecular Cobalt Tetraazamacrocycles. *Journal of the American Chemical Society* **2012**, *134* (6), 3164–3170. https://doi.org/10.1021/ja210661k.

(46) Nie, C.; Liu, C.; Gong, L.; Wang, M. Boosting the Performance of a Silicon Photocathode for Photoelectrochemical Hydrogen Production by Immobilization of a Cobalt Tetraazamacrocyclic Catalyst. *Journal of Materials Chemistry A* **2020**, *5* (45), 23566–23576. https://doi.org/10.1039/D0TA09942B.

(47) Cheng, X.; Sun, S.; Liang, M.; Shi, Y.; Sun, Z.; Xue, S. Organic Dyes Incorporating the Cyclopentadithiophene Moiety for Efficient Dye-Sensitized Solar Cells. *Dyes and Pigments* **2012**, *92* (3), 1292–1299. https://doi.org/10.1016/j.dyepig.2011.09.019.

(48) Massin, J.; Bräutigam, M.; Kaeffer, N.; Queyriaux, N.; Field, M. J.; Schacher, F. H.; Popp, J.; Chavarot-Kerlidou, M.; Dietzek, B.; Artero, V. Dye-Sensitized PS-b-P2VP-Templated Nickel Oxide Films for Photoelectrochemical Applications. *Interface Focus* **2015**, *5* (3), 20140083. https://doi.org/10.1098/rsfs.2014.0083.

(49) Ji, Z.; Natu, G.; Huang, Z.; Wu, Y. Linker Effect in Organic Donor-Acceptor Dyes for p-Type NiO Dye Sensitized Solar Cells. *Energy and Environmental Science* **2011**, *4* (8), 2818–2821. https://doi.org/10.1039/c1ee01527c.

(50) Ishow, E.; Clavier, G.; Miomandre, F.; Rebarz, M.; Buntinx, G.; Poizat, O. Comprehensive Investigation of the Excited-State Dynamics of Push–Pull Triphenylamine Dyes as Models for

Photonic Applications. *Physical Chemistry Chemical Physics* **2013**, *15* (33), 13922. https://doi.org/10.1039/c3cp51480c.

(51) Zieschang, F.; Schreck, M. H.; Schmiedel, A.; Holzapfel, M.; Klein, J. H.; Walter, C.; Engels, B.; Lambert, C. Photoinduced Electron Transfer Dynamics in Triarylamine-Naphthalene Diimide Cascades. *Journal of Physical Chemistry C* **2014**, *118* (48), 27698–27714. https://doi.org/10.1021/jp5085058.

(52) de Miguel, G.; Wielopolski, M.; Schuster, D. I.; Fazio, M. A.; Lee, O. P.; Haley, C. K.; Ortiz, A. L.; Echegoyen, L.; Clark, T.; Guldi, D. M. Triazole Bridges as Versatile Linkers in Electron Donor–Acceptor Conjugates. *Journal of the American Chemical Society* **2011**, *133* (33), 13036–13054. https://doi.org/10.1021/ja202485s.

(53) Sheth, S.; Baron, A.; Herrero, C.; Vauzeilles, B.; Aukauloo, A.; Leibl, W. Light-Induced Tryptophan Radical Generation in a Click Modular Assembly of a Sensitiser-Tryptophan Residue. *Photochemical & Photobiological Sciences* **2013**, *12* (6), 1074. https://doi.org/10.1039/c3pp50021g.

(54) Baron, A.; Herrero, C.; Quaranta, A.; Charlot, M.-F.; Leibl, W.; Vauzeilles, B.; Aukauloo, A. Click Chemistry on a Ruthenium Polypyridine Complex. An Efficient and Versatile Synthetic Route for the Synthesis of Photoactive Modular Assemblies. *Inorganic Chemistry* **2012**, *51* (11), 5985–5987. https://doi.org/10.1021/ic300227j.

(55) Baron, A.; Herrero, C.; Quaranta, A.; Charlot, M.-F.; Leibl, W.; Vauzeilles, B.; Aukauloo, A. Efficient Electron Transfer through a Triazole Link in Ruthenium(II) Polypyridine Type Complexes. *Chemical Communications* **2011**, *47* (39), 11011. https://doi.org/10.1039/c1cc13683f.

(56) Queyriaux, N.; Andreiadis, E. S.; Torelli, S.; Pecaut, J.; Veldkamp, B. S.; Margulies, E. A.; Wasielewski, M. R.; Chavarot-Kerlidou, M.; Artero, V. CuAAC-Based Assembly and Characterization of a Ruthenium–Copper Dyad Containing a Diimine–Dioxime Ligand Framework. *Faraday Discussions* **2017**, *198*, 251–261. https://doi.org/10.1039/C6FD00204H.

(57) Li, N.; Gibson, E. A.; Qin, P.; Boschloo, G.; Gorlov, M.; Hagfeldt, A.; Sun, L. Double-Layered NiO Photocathodes for p-Type DSSCs with Record IPCE. *Advanced Materials* **2010**, *22* (15), 1759–1762. https://doi.org/10.1002/adma.200903151.

(58) Sumikura, S.; Mori, S.; Shimizu, S.; Usami, H.; Suzuki, E. Syntheses of NiO Nanoporous Films Using Nonionic Triblock Co-Polymer Templates and Their Application to Photo-Cathodes of p-Type Dye-Sensitized Solar Cells. *Journal of Photochemistry and Photobiology A: Chemistry* **2008**, *199* (1), 1–7. https://doi.org/10.1016/j.jphotochem.2008.04.007.

(59) Ameline, D.; Diring, S.; Farre, Y.; Pellegrin, Y.; Naponiello, G.; Blart, E.; Charrier, B.; Dini, D.; Jacquemin, D.; Odobel, F. Isoindigo Derivatives for Application in P-Type Dye Sensitized Solar Cells. *RSC Advances* **2015**, *5* (104), 85530–85539. https://doi.org/10.1039/C5RA11744E.

(60) Boschloo, G.; Hagfeldt, A. Spectroelectrochemistry of Nanostructured NiO. *Journal of Physical Chemistry B* **2001**, *105* (15), 3039–3044. https://doi.org/10.1021/jp003499s.

(61) Kirner, J. T.; Stracke, J. J.; Gregg, B. A.; Finke, R. G. Visible-Light-Assisted Photoelectrochemical Water Oxidation by Thin Films of a Phosphonate-Functionalized Perylene Diimide Plus CoO x Cocatalyst. *ACS Applied Materials & Interfaces* **2014**, *6* (16), 13367–13377. https://doi.org/10.1021/am405598w.

(62) Sonavane, A. C.; Inamdar, A. I.; Shinde, P. S.; Deshmukh, H. P.; Patil, R. S.; Patil, P. S. Efficient Electrochromic Nickel Oxide Thin Films by Electrodeposition. *J. Alloys Compd.* **2010**, *489* (2), 667–673. https://doi.org/10.1016/j.jallcom.2009.09.146.

(63) Xia, X. H.; Tu, J. P.; Zhang, J.; Wang, X. L.; Zhang, W. K.; Huang, H. Electrochromic Properties of Porous NiO Thin Films Prepared by a Chemical Bath Deposition. *Sol. Energ. Mat. Sol. C.* **2008**, *92* (6), 628–633. https://doi.org/10.1016/j.solmat.2008.01.009.

(64) Zietz, B.; Gabrielsson, E.; Johansson, V.; El-Zohry, A. M.; Sun, L.; Kloo, L. Photoisomerization of the Cyanoacrylic Acid Acceptor Group – a Potential Problem for Organic Dyes in Solar Cells. *Physical Chemistry Chemical Physics* **2014**, *16* (6), 2251. https://doi.org/10.1039/c3cp54048k.

(65) Queyriaux, N.; Wahyuono, R. A.; Fize, J.; Gablin, C.; Wächtler, M.; Martinez, E.; Léonard, D.; Dietzek, B.; Artero, V.; Chavarot-Kerlidou, M. Aqueous Photocurrent Measurements Correlated to Ultrafast Electron Transfer Dynamics at Ruthenium Tris Diimine Sensitized NiO Photocathodes. *The Journal of Physical Chemistry C* **2017**, *121* (11), 5891–5904. https://doi.org/10.1021/acs.jpcc.6b12536.

(66) Bräutigam, M.; Kübel, J.; Schulz, M.; Vos, J. G.; Dietzek, B. Hole Injection Dynamics from Two Structurally Related Ru–Bipyridine Complexes into NiOx Is Determined by the Substitution Pattern of the Ligands. *Physical Chemistry Chemical Physics* **2015**, *17* (12), 7823–7830. https://doi.org/10.1039/C4CP05663A.

(67) Han, Y.; Dillon, R. J.; Flynn, C. J.; Rountree, E. S.; Alibabaei, L.; Cahoon, J. F.; Papanikolas, J. M.; Dempsey, J. L. Interfacial Electron Transfer Yields in Dye-Sensitized NiO Photocathodes Correlated to Excited-State Dipole Orientation of Ruthenium Chromophores. *Canadian Journal of Chemistry* **2018**, *96* (9), 865–874. https://doi.org/10.1139/cjc-2017-0359.

(68) Kou, Y.; Nakatani, S.; Sunagawa, G.; Tachikawa, Y.; Masui, D.; Shimada, T.; Takagi, S.; Tryk, D. A.; Nabetani, Y.; Tachibana, H.; Inoue, H. Visible Light-Induced Reduction of Carbon Dioxide Sensitized by a Porphyrin-Rhenium Dyad Metal Complex on p-Type Semiconducting NiO as the Reduction Terminal End of an Artificial Photosynthetic System. *Journal of Catalysis* **2014**, *310*, 57–66. https://doi.org/10.1016/j.jcat.2013.03.025.

(69) Daeneke, T.; Yu, Z.; Lee, G. P.; Fu, D.; Duffy, N. W.; Makuta, S.; Tachibana, Y.; Spiccia, L.; Mishra, A.; Bäuerle, P.; Bach, U. Dominating Energy Losses in NiO P-Type Dye-Sensitized Solar Cells. *Advanced Energy Materials* **2015**, *5* (4). https://doi.org/10.1002/aenm.201401387.

(70) Bold, S.; Straistari, T.; Muñoz-García, A. B.; Pavone, M.; Artero, V.; Chavarot-Kerlidou, M.; Dietzek, B. Investigating Light-Induced Processes in Covalent Dye-Catalyst Assemblies for Hydrogen Production. *Catalysts* **2020**, *10* (11), 1340. https://doi.org/10.3390/catal10111340.

(71) Massin, J.; Bräutigam, M.; Bold, S.; Wächtler, M.; Pavone, M.; Muñoz-García, A. B.; Dietzek, B.; Artero, V.; Chavarot-Kerlidou, M. Investigating Light-Driven Hole Injection and Hydrogen Evolution Catalysis at Dye-Sensitized NiO Photocathodes: A Combined Experimental–Theoretical Study. *The Journal of Physical Chemistry C* **2019**, *123* (28), 17176–17184. https://doi.org/10.1021/acs.jpcc.9b04715.

(72) Black, F. A.; Clark, C. A.; Summers, G. H.; Clark, I. P.; Towrie, M.; Penfold, T.; George, M. W.; Gibson, E. A. Investigating Interfacial Electron Transfer in Dye-Sensitized NiO Using Vibrational Spectroscopy. *Physical Chemistry Chemical Physics* **2017**, *19* (11), 7877–7885. https://doi.org/10.1039/C6CP05712H.

(73) Morandeira, A.; Boschloo, G.; Hagfeldt, A.; Hammarström, L. Coumarin 343-NiO Films as Nanostructured Photocathodes in Dye-Sensitized Solar Cells: Ultrafast Electron Transfer, Effect of the I3/I - Redox Couple and Mechanism of Photocurrent Generation. *Journal of Physical Chemistry C* **2008**, *112* (25), 9530–9537. https://doi.org/10.1021/jp800760q.

(74) Morandeira, A.; Boschloo, G.; Hagfeldt, A.; Hammarström, L. Photoinduced Ultrafast Dynamics of Coumarin 343 Sensitized P-Type-Nanostructured NiO Films. *The Journal of Physical Chemistry B* **2005**, *109* (41), 19403–19410. https://doi.org/10.1021/jp053230e.

(75) Sheibani, E.; Zhang, L.; Liu, P.; Xu, B.; Mijangos, E.; Boschloo, G.; Hagfeldt, A.; Hammarström, L.; Kloo, L.; Tian, H. A Study of Oligothiophene–Acceptor Dyes in p-Type Dye-Sensitized Solar Cells. *RSC Advances* **2016**, *6* (22), 18165–18177. https://doi.org/10.1039/C5RA26310G.

(76) Smeigh, A. L.; le Pleux, L.; Fortage, J.; Pellegrin, Y.; Blart, E.; Odobel, F.; Hammarström, L. Ultrafast Recombination for NiO Sensitized with a Series of Perylene Imide Sensitizers Exhibiting Marcus Normal Behaviour. *Chemical Communications* **2012**, *48* (5), 678–680. https://doi.org/10.1039/c1cc16144j.

(77) Gibson, E. A.; Smeigh, A. L.; le Pleux, L.; Fortage, J.; Boschloo, G.; Blart, E.; Pellegrin, Y.; Odobel, F.; Hagfeldt, A.; Hammarström, L. A P-Type NiO-Based Dye-Sensitized Solar Cell with an Open-Circuit Voltage of 0.35 V. *Angewandte Chemie International Edition* **2009**, *48* (24), 4402–4405. https://doi.org/10.1002/anie.200900423.

(78) le Pleux, L.; Smeigh, A. L.; Gibson, E.; Pellegrin, Y.; Blart, E.; Boschloo, G.; Hagfeldt, A.; Hammarström, L.; Odobel, F. Synthesis, Photophysical and Photovoltaic Investigations of Acceptor-Functionalized Perylene Monoimide Dyes for Nickel Oxide p-Type Dye-Sensitized Solar Cells. *Energy and Environmental Science* **2011**, *4* (6), 2075–2084. https://doi.org/10.1039/c1ee01148k.

(79) Yu, Y.; Click, K. A.; Polen, S. M.; He, M.; Hadad, C. M.; Wu, Y. Electron Transfer Kinetics of a Series of Bilayer Triphenylamine-Oligothiophene-Perylenemonoimide Sensitizers for Dye-Sensitized NiO. *Journal of Physical Chemistry C* **2017**, *121* (38), 20720–20728. https://doi.org/10.1021/acs.jpcc.7b07859.

(80) Flender, O.; Scholz, M.; Klein, J. R.; Oum, K.; Lenzer, T. Excited-State Relaxation of the Solar Cell Dye D49 in Organic Solvents and on Mesoporous Al 2 O 3 and TiO 2 Thin Films. *Physical Chemistry Chemical Physics* **2016**, *18* (37), 26010–26019. https://doi.org/10.1039/C6CP05167G.

(81) Zhu, H.; Wang, X.; Ma, R.; Kuang, Z.; Guo, Q.; Xia, A. Intramolecular Charge Transfer and Solvation of Photoactive Molecules with Conjugated Push–Pull Structures. *ChemPhysChem* **2016**, *17* (20), 3245–3251. https://doi.org/10.1002/cphc.201600674.

(82) Ishow, E.; Guillot, R.; Buntinx, G.; Poizat, O. Photoinduced Intramolecular Charge-Transfer Dynamics of a Red-Emitting Dicyanovinyl-Based Triarylamine Dye in Solution. *Journal of Photochemistry and Photobiology A: Chemistry* **2012**, *234*, 27–36. https://doi.org/10.1016/j.jphotochem.2011.12.018.

(83) Gatty, M. G.; Pullen, S.; Sheibani, E.; Tian, H.; Ott, S.; Hammarström, L. Direct Evidence of Catalyst Reduction on Dye and Catalyst Co-Sensitized NiO Photocathodes by Mid-Infrared Transient Absorption Spectroscopy. *Chemical Science* **2018**, *9* (22), 4983–4991. https://doi.org/10.1039/C8SC00990B.

(84) Morandeira, A.; Fortage, J.; Edvinsson, T.; Pleux, L. le; Blart, E.; Boschloo, G.; Hagfeldt, A.; Hammarström, L.; Odobel, F. Improved Photon-to-Current Conversion Efficiency with a Nanoporous p-Type NiO Electrode by the Use of a Sensitizer-Acceptor Dyad. *Journal of Physical Chemistry C* **2008**, *112* (5), 1721–1728. https://doi.org/10.1021/jp077446n.

(85) Qin, P.; Wiberg, J.; Gibson, E. A.; Linder, M.; Li, L.; Brinck, T.; Hagfeldt, A.; Albinsson, B.; Sun, L. Synthesis and Mechanistic Studies of Organic Chromophores with Different Energy Levels for P-Type Dye-Sensitized Solar Cells. *The Journal of Physical Chemistry C* **2010**, *114* (10), 4738–4748. https://doi.org/10.1021/jp911091n.

(86) Põldme, N.; O'Reilly, L.; Fletcher, I.; Portoles, J.; Sazanovich, I. v; Towrie, M.; Long, C.; Vos, J. G.; Pryce, M. T.; Gibson, E. A. Photoelectrocatalytic H2 Evolution from Integrated Photocatalysts Adsorbed on NiO. *Chemical Science* **2019**, *10* (1), 99–112. https://doi.org/10.1039/C8SC02575D.

(87) Gardner, J. M.; Beyler, M.; Karnahl, M.; Tschierlei, S.; Ott, S.; Hammarström, L. Light-Driven Electron Transfer between a Photosensitizer and a Proton-Reducing Catalyst Co-Adsorbed to NiO. *Journal of the American Chemical Society* **2012**, *134* (47), 19322–19325. https://doi.org/10.1021/ja3082268.

(88) Queyriaux, N.; Sun, D.; Fize, J.; Pécaut, J.; Field, M. J.; Chavarot-Kerlidou, M.; Artero, V. Electrocatalytic Hydrogen Evolution with a Cobalt Complex Bearing Pendant Proton Relays: Acid Strength and Applied Potential Govern Mechanism and Stability. *Journal of the American Chemical Society* **2020**, *142* (1), 274–282. https://doi.org/10.1021/jacs.9b10407.

(89) Queyriaux, N.; Jane, R. T.; Massin, J.; Artero, V.; Chavarot-Kerlidou, M. Recent Developments in Hydrogen Evolving Molecular Cobalt(II)-Polypyridyl Catalysts. *Coordination Chemistry Reviews* **2015**, *304–305*, 3–19. https://doi.org/10.1016/j.ccr.2015.03.014.

(90) Queyriaux, N.; Giannoudis, E.; Windle, C. D.; Roy, S.; Pécaut, J.; Coutsolelos, A. G.; Artero, V.; Chavarot-Kerlidou, M. A Noble Metal-Free Photocatalytic System Based on a Novel Cobalt Tetrapyridyl Catalyst for Hydrogen Production in Fully Aqueous Medium. *Sustainable Energy Fuels* **2018**, *25* (2), 553–557. https://doi.org/10.1039/c7se00428a.

(91) Zee, D. Z.; Chantarojsiri, T.; Long, J. R.; Chang, C. J. Metal–Polypyridyl Catalysts for Electro- and Photochemical Reduction of Water to Hydrogen. *Accounts of Chemical Research* **2015**, *48* (7), 2027–2036. https://doi.org/10.1021/acs.accounts.5b00082.

(92) Materna, K. L.; Beiler, A. M.; Thapper, A.; Ott, S.; Tian, H.; Hammarström, L. Understanding the Performance of NiO Photocathodes with Alkyl-Derivatized Cobalt Catalysts and a Push–Pull Dye. *ACS Applied Materials & Interfaces* **2020**, *12* (28), 31372–31381. https://doi.org/10.1021/acsami.0c05228.

(93) Kaeffer, N.; Chavarot-Kerlidou, M.; Artero, V. Hydrogen Evolution Catalyzed by Cobalt Diimine-Dioxime Complexes. *Accounts of Chemical Research* **2015**, *48* (5), 1286–1295. https://doi.org/10.1021/acs.accounts.5b00058.

(94) Kaeffer, N.; Morozan, A.; Fize, J.; Martinez, E.; Guetaz, L.; Artero, V. The Dark Side of Molecular Catalysis: Diimine–Dioxime Cobalt Complexes Are Not the Actual Hydrogen Evolution Electrocatalyst in Acidic Aqueous Solutions. *ACS Catalysis* **2016**, *6* (6), 3727–3737. https://doi.org/10.1021/acscatal.6b00378.

(95) Anxolabéhère-Mallart, E.; Costentin, C.; Fournier, M.; Nowak, S.; Robert, M.; Savéant, J.-M. Boron-Capped Tris(Glyoximato) Cobalt Clathrochelate as a Precursor for the Electrodeposition

of Nanoparticles Catalyzing H2 Evolution in Water. *Journal of the American Chemical Society* **2012**, *134* (14), 6104–6107. https://doi.org/10.1021/ja301134e.

(96) Cobo, S.; Heidkamp, J.; Jacques, P.-A.; Fize, J.; Fourmond, V.; Guetaz, L.; Jousselme, B.; Ivanova, V.; Dau, H.; Palacin, S.; Fontecave, M.; Artero, V. A Janus Cobalt-Based Catalytic Material for Electro-Splitting of Water. *Nature Materials* **2012**, *11* (9), 802–807. https://doi.org/10.1038/nmat3385.

(97) Andreiadis, E. S.; Jacques, P.-A.; Tran, P. D.; Leyris, A.; Chavarot-Kerlidou, M.; Jousselme, B.; Matheron, M.; Pécaut, J.; Palacin, S.; Fontecave, M.; Artero, V. Molecular Engineering of a Cobalt-Based Electrocatalytic Nanomaterial for H2 Evolution under Fully Aqueous Conditions. *Nature Chemistry* **2013**, *5* (1), 48–53. https://doi.org/10.1038/nchem.1481.

(98) Lee, D. K.; Lee, D.; Lumley, M. A.; Choi, K. S. Progress on Ternary Oxide-Based Photoanodes for Use in Photoelectrochemical Cells for Solar Water Splitting. *Chemical Society Reviews* **2019**, *48* (7), 2126–2157. https://doi.org/10.1039/c8cs00761f.

(99) Sahara, G.; Kumagai, H.; Maeda, K.; Kaeffer, N.; Artero, V.; Higashi, M.; Abe, R.; Ishitani, O. Photoelectrochemical Reduction of CO2 Coupled to Water Oxidation Using a Photocathode with a Ru(II)–Re(I) Complex Photocatalyst and a CoOx /TaON Photoanode. *Journal of the American Chemical Society* **2016**, *138* (42), 14152–14158. https://doi.org/10.1021/jacs.6b09212.

(100) Li, T. T.; Shan, B.; Meyer, T. J. Stable Molecular Photocathode for Solar-Driven CO2 Reduction in Aqueous Solutions. *ACS Energy Letters* **2019**, *4* (3), 629–636. https://doi.org/10.1021/acsenergylett.8b02512.

(101) Cheshire, T. P.; Brennaman, M. K.; Giokas, P. G.; Zigler, D. F.; Moran, A. M.; Papanikolas, J. M.; Meyer, G. J.; Meyer, T. J.; Houle, F. A. Ultrafast Relaxations in Ruthenium Polypyridyl Chromophores Determined by Stochastic Kinetics Simulations. *The Journal of Physical Chemistry B* **2020**, *124* (28), 5971–5985. https://doi.org/10.1021/acs.jpcb.0c03110.

(102) Tebo, A. G.; Quaranta, A.; Herrero, C.; Pecoraro, V. L.; Aukauloo, A. Intramolecular Photogeneration of a Tyrosine Radical in a Designed Protein. *ChemPhotoChem* **2017**, *1* (3), 89–92. https://doi.org/10.1002/cptc.201600044.

(103) Herrero, C.; Quaranta, A.; el Ghachtouli, S.; Vauzeilles, B.; Leibl, W.; Aukauloo, A. Carbon Dioxide Reduction via Light Activation of a Ruthenium-Ni(Cyclam) Complex. *Physical Chemistry Chemical Physics* **2014**, *16* (24), 12067–12072. https://doi.org/10.1039/c3cp54946a.

(104) Herrero, C.; Quaranta, A.; Sircoglou, M.; Sénéchal-David, K.; Baron, A.; Marín, I. M.; Buron, C.; Baltaze, J.-P.; Leibl, W.; Aukauloo, A.; Banse, F. Successive Light-Induced Two Electron Transfers in a Ru–Fe Supramolecular Assembly: From Ru–Fe(II)–OH2 to Ru–Fe(IV)–Oxo. *Chemical Science* **2015**, *6* (4), 2323–2327. https://doi.org/10.1039/C5SC00024F.

(105) Herrero, C.; Batchelor, L.; Baron, A.; el Ghachtouli, S.; Sheth, S.; Guillot, R.; Vauzeilles, B.; Sircoglou, M.; Mallah, T.; Leibl, W.; Aukauloo, A. Click Chemistry as a Convenient Tool for the Incorporation of a Ruthenium Chromophore and a Nickel-Salen Monomer into a Visible-Light-Active Assembly. *European Journal of Inorganic Chemistry* **2013**, *2013* (4), 494–499. https://doi.org/10.1002/ejic.201201161.

(106) Brown, A. M.; Antila, L. J.; Mirmohades, M.; Pullen, S.; Ott, S.; Hammarström, L. Ultrafast Electron Transfer Between Dye and Catalyst on a Mesoporous NiO Surface. *Journal of the American Chemical Society* **2016**, *138* (26), 8060–8063. https://doi.org/10.1021/jacs.6b03889.

(107) Dalle, K. E.; Warnan, J.; Leung, J. J.; Reuillard, B.; Karmel, I. S.; Reisner, E. Electro- and Solar-Driven Fuel Synthesis with First Row Transition Metal Complexes. *Chemical Reviews* **2019**, *119* (4), 2752–2875. https://doi.org/10.1021/acs.chemrev.8b00392.

(108) Xu, P.; McCool, N. S.; Mallouk, T. E. Water Splitting Dye-Sensitized Solar Cells. *Nano Today* **2017**, *14*, 42–58. https://doi.org/10.1016/j.nantod.2017.04.009.

(109) Tong, L.; Duan, L.; Zhou, A.; Thummel, R. P. First-Row Transition Metal Polypyridine Complexes That Catalyze Proton to Hydrogen Reduction. *Coordination Chemistry Reviews* **2020**, *402*, 213079. https://doi.org/10.1016/j.ccr.2019.213079.

(110) O'Reilly, J. E. Oxidation-Reduction Potential of the Ferro-Ferricyanide System in Buffer Solutions. *Biochimica et Biophysica Acta (BBA) - Bioenergetics* **1973**, *292* (3), 509–515. https://doi.org/10.1016/0005-2728(73)90001-7.

(111) Karnahl, M.; Kuhnt, C.; Ma, F.; Yartsev, A.; Schmitt, M.; Dietzek, B.; Rau, S.; Popp, J. Tuning of Photocatalytic Hydrogen Production and Photoinduced Intramolecular Electron Transfer Rates by Regioselective Bridging Ligand Substitution. *ChemPhysChem* **2011**, *12* (11), 2101–2109. https://doi.org/10.1002/cphc.201100245.

(112) Dietzek, B.; Pascher, T.; Sundström, V.; Yartsev, A. Appearance of Coherent Artifact Signals in Femtosecond Transient Absorption Spectroscopy in Dependence on Detector Design. *Laser Physics Letters* **2007**, *4* (1), 38–43. https://doi.org/10.1002/lapl.200610070.

(113) Sittig, M.; Schmidt, B.; Görls, H.; Bocklitz, T.; Wächtler, M.; Zechel, S.; Hager, M. D.; Dietzek, B. Fluorescence Upconversion by Triplet–Triplet Annihilation in All-Organic Poly(Methacrylate)-Terpolymers. *Physical Chemistry Chemical Physics* **2020**, *22* (7), 4072–4079. https://doi.org/10.1039/D0CP00232A.

Table of content (TOC) figure: